Mapping regulatory networks underlying *Leishmania* stage differentiation reveals an essential role for protein degradation in parasite development

Pascale Pescher[1*], Thibaut Douché[2], Quentin Giai-Gianetto[2,3], Karen Druart[2], Julie Kovarova[5], Blaise Li[3], Caroline Proux[4], Rachel Legendre[3,4], Hugo Varet[3,4], K Shanmugha Rajan[7,8], Laura Piel[1], Céline Besse[6], Anne Boland[6], Jean-François Deleuze[6], Mariette Matondo[2], Michael P. Barrett[5], Shulamit Michaeli[8] and Gerald F. Späth[1*]

[1]Institut Pasteur, Université Paris Cité, INSERM 1201, Unité de Parasitologie moléculaire et Signalisation, Paris, France, [2]Institut Pasteur, Université Paris Cité, CNRS UAR 2024, Proteomic Platform, Mass Spectrometry for Biology Unit, Paris, France , [3]Institut Pasteur, Université Paris Cité, Biostatistics and Bioinformatics Hub, Paris, France, [4]Institut Pasteur, Université Paris Cité, Pôle Biomics, [5]Glasgow Centre for Parasitology, University of Glasgow, Glasgow, UK, [6]Université Paris-Saclay, CEA, Centre National de Recherche en Génomique Humaine, Evry, France, [7]Weizmann Institute of Science, Department of Chemical and Structural Biology, Rehovot, Israel, [8]Bar-Ilan University, Mina and Everard Goodman Faculty of Life Sciences and Advanced and Nanotechnology Institute, Ramat-Gan, Israel.

*co-corresponding authors

Correspondence: pascale.pescher@pasteur.fr, gerald.spaeth@pasteur.fr

Keywords: *Leishmania donovani*, stage differentiation, systems analysis, protein degradation, regulatory networks

ABSTRACT

Genetic feedback control represents a central paradigm in regulation of biological systems and their response to environmental change. Vector-borne pathogens have evolved complex developmental programs to adapt to very distinct host environments, but the relevance of feedback regulation in stage differentiation remains to be elucidated. Here we address this open question in the trypanosomatid parasite *Leishmania* that shows constitutive gene transcription, thus providing a unique model system to assess post-transcriptional mechanisms of feedback regulation in the absence of confounding transcriptional control. Using a five-layer integrative systems analysis (from genome to metabolome), we examined hamster-isolated *Leishmania donovani* amastigotes and culture-derived insect-stage promastigotes. This approach enabled us to rule out genomic adaptation as a driver of parasite stage differentiation, confirm the pivotal role of differential mRNA turnover in stage-specific gene expression, and uncover an unexpectedly broad dynamic range of protein abundance changes that correlated poorly with transcript levels. This discrepancy was attributed to (i) stage-specific translational control, as indicated by alterations in snoRNA expression and changes in rRNA modification they guide, and (ii) differential protein degradation, as revealed by quantitative proteomics of parasites treated with the proteasomal inhibitor lactacystin. Notably, lactacystin treatment stalled the transition of spleen-derived amastigotes into promastigotes in culture, further underscoring the role of proteasomal activity in stage differentiation. Integration of our five-layer systems analysis established the first link between *Leishmania* development and the expression of highly connected, stage-specific regulatory networks encompassing mRNA turnover, protein translation, phosphorylation, and degradation. These networks engage in complex recursive (self-regulating) interactions involved in post-transcriptional regulation, ribosomal biogenesis, and signal transduction, as well as reciprocal (cross-regulating) interactions, including a network between protein kinases that phosphorylate proteasomal components in a stage-specific manner and proteasomal activities that, in turn, target protein kinases for stage-specific degradation. Our findings provide a powerful experimental framework to dissect the emergent properties of these regulatory feedback loops, offering critical

27 insights into intracellular infection and serving as a blueprint for other vector-borne pathogens that rely
28 on disease-associated developmental transitions.
29
30 **INTRODUCTION**
31 During their infectious cycle, many protist and fungal pathogens undergo complex developmental
32 transitions that adapt their biology to different host environments, thus ensuring transmission,
33 persistence or immune evasion. For example, stage differentiation of the malarial parasite *Plasmodium*
34 spp is tightly controlled at transcriptional levels by the dynamic interplay between epigenetic regulators
35 that remodel the chromatin landscape to accommodate stage-specific transcription factors, such as AP2
36 DNA-binding family members (1, 2). Likewise, the transition from fast-growing tachyzoites to slow-
37 growing bradyzoites during mammalian *Toxoplasma* infection is regulated by the single master TF
38 BFD1 (3). Unlike these apicomplexan parasites, stage-differentiation in the trypanosomatid pathogen
39 *Leishmania* spp is not regulated at the level of transcriptional control, raising the question of how these
40 parasites establish and maintain the various adaptive forms that develop inside their insect and
41 mammalian hosts.
42 *Leishmania* spp are protist parasites of humans that represent a global public health problem
43 causing a series of immunopathologies termed the leishmaniases (4-7). These parasites differentiate
44 into various developmental forms that are adapted for extracellular proliferation inside the sand fly
45 midgut (procyclic promastigotes), transmission from the vector to the mammalian host during uptake
46 of a blood meal (metacyclic promastigotes), and intracellular proliferation inside fully acidified
47 macrophage phagolysosomes (amastigotes) (8). Unlike other eukaryotes, *Leishmania* development is
48 not controlled transcriptionally as protein-coding genes in these parasites lack individual promoters and
49 are constitutively transcribed at all stages involving parasite-specific processes such as polycistronic
50 transcription and trans-splicing (9, 10). Despite the largely constitutive gene transcription, different
51 *Leishmania* stages are characterized by striking morphological, biochemical and metabolic changes
52 (11-16), and these are regulated by a plethora of post-transcriptional mechanisms, including differential
53 mRNA turn over through the binding of various proteins and protein complexes to the 5' and 3'
54 untranslated regions (UTRs)(17-22), that can trigger mRNA degradation via deadenylation and

55 decapping (23, 24). Differential gene expression in *Leishmania* can further be regulated at the
56 translational level, for example through (i) binding to the 5' UTR of one of the six isoforms of the
57 *Leishmania* cap-binding protein eIF4E that may confer selective ribosome recruitment, (ii) the
58 recruitment of Poly(A) Binding Protein 1 (PABP1) to the 3' UTR promoting translation by stabilizing
59 the poly(A) tail, or (iii) the differential expression of ribosomal proteins that can increase the landscape
60 of specialized ribosomes (25-34). Finally, differential gene expression in *Leishmania* can also be
61 controlled at the level of protein stability, through stage-specific expression of proteasomal components,
62 autophagy-related genes (ATGs) or lysosomal proteases (35-41).

63 While each level of gene expression control has been studied individually in different
64 *Leishmania* species, how these different types of regulation are integrated during *Leishmania* stage
65 differentiation remains to be elucidated. Here, we address this open question by applying a 5-layer,
66 systems level analysis on the two major life cycle stages of *Leishmania donovani*, i.e. hamster-isolated,
67 *bona-fide* amastigotes and derived promastigotes. Our analysis draws a complex picture of the
68 *Leishmania* differentiation process that emerges from the interactions between recursive (i.e. self-
69 controlling) and reciprocal (i.e. cross-controlling) feedback loops between mRNA turnover, protein
70 translation, protein phosphorylation and protein degradation. Our data reveal *Leishmania* as an
71 interesting model system to analyze phenotypic adaptation in the absence of transcriptional control and
72 to dissociate the role of complex regulatory networks in the development of stable, disease-causing life
73 cycle stages in eukaryotic pathogens.
74
75

76 **MATERIAL & METHODS**

77 **Ethics statement.** Work on animals was performed in compliance with French and European
78 regulations on care and protection of laboratory animals (EC Directive 2010/63, French Law 2013-118,
79 February 6th, 2013). All animal experiments were approved by the Ethics Committee and the Animal
80 welfare body of Institut Pasteur and by the Ministère de l'Enseignement Supérieur, de la Recherche et
81 de l'Innovation (project n°#19683).

82

83 **Animals.** Twenty one female Golden Syrian hamsters (*Mesocricetus auratus* RjHan:AURA, weighting
84 between 50 – 60 g) were purchased from Janvier Laboratories. All animals were handled under specific,
85 pathogen-free conditions in biohazard level 3 animal facilities (A3) accredited by the French Ministry
86 of Agriculture for performing experiments on live rodents (agreement A75-15-01).

87

88 **Parasites and culture.** *Leishmania donovani* strain 1S2D (MHOM/SD/62/1S-CL2D) was obtained
89 from Henry Murray, Weill Cornell Medical College, New York, USA and maintained by serial passages
90 in hamsters. Anesthetized hamsters were inoculated by intra-cardiac injection of $5x10^7$ amastigotes
91 purified from hamster infected spleens as described previously (42). The weight of the animals was
92 recorded over time, and the animals were euthanized by CO_2 asphyxiation before they reached the end-
93 point of infection represented by a 20% loss of body weight. Amastigotes were then recovered from the
94 infected hamster spleens and used for nucleic acid and protein extractions, or differentiated into
95 promastigotes at 26°C in M199 complete medium (M199, 10% FBS, 25 mM HEPES; 100 µM adenine,
96 2 mM L-glutamine, 10 µg/ml folic acid, 13.7 µM hemin, 4.2 mM $NaHCO_3$, 1xRPMI1640 vitamins, 8
97 µM 6-biopterin, 100 units penicillin and 100 µg/ml streptomycin, pH 7.4). Promastigotes, derived from
98 splenic amastigotes, were collected after 2 *in vitro* passages for nucleic acid and protein extractions.

99

100 **Experimental design.** Strains issued from independent experimental evolution assays are identified by
101 number, e.g. amastigote ama1 and promastigote pro1 are the parasites prepared from hamster H1 (see
102 Figures 1A and S1 for details). For comparative analyses, DNA, RNA, proteins and metabolites were

103 extracted from different splenic ama and their matching pro parasites, the latter being collected for
104 extraction during exponential growth phase.
105
106 **Parasite differentiation and lactacystin treatment.** Spleen-derived amastigotes were incubated at
107 $2x10^7$/ml and 26°C in presence or absence of 10 µM of lactacystin (L6785, Sigma) for 3, 6, 18 and 48h
108 in M199 complete medium. At each time point, parasites were collected to control for the presence of
109 paraflagellar rod protein 2 (PFR2) as promastigote differentiation marker. After one *in vitro* passage,
110 amastigote-derived promastigotes were incubated at a concentration of $2x10^7$ parasites per ml in
111 presence or absence of 10 µM of lactacystin for 18h. Parasite viability was assessed by FACS analysis
112 after 18h of treatment by propidium iodide (1µg/ml) or YO-PRO-1 (0.2 µM) (# Y3603, Invitrogen)
113 staining as readout. Parasites were collected from 25 ml of culture after 18h of treatment for
114 quantitative, label-free proteomics analyses.

115 **Microscopy.** Differential interference contrast (DIC) microscopy was applied on hamster-derived
116 amastigotes during *in vitro* differentiation to promastigotes using an Axioplan 2 imaging microscope
117 using a 63x oil immersion objective, the AxioVision Rel.4.8 software and an AxioCam MRm camera
118 (Carl Zeiss). Alternatively, microscopic images of amastigotes in presence or absence of the lactacystin
119 inhibitor were obtained using the EVOS FL microscope (life technologies) at a 20x magnification.

120 **Western blot analysis.** Protein extracts were obtained from parasites after 3, 6, 18 and 48h of
121 differentiation from amastigotes to promastigotes in presence or absence of lactacystin. Extracts were
122 loaded on 4-12% SDS-PAGE (NuPage 4-12% Bis-Tris gel NP0321BOX, Invitrogen), separated by
123 electrophoresis and stained with Coomassie blue or transferred onto PVDF membrane. The presence of
124 PFR2 and α-tubulin was revealed using the anti-PFR2 antibody (kindly given by Philippe Bastin), an
125 anti- α-tubulin antibody (clone B-5-1-2, Sigma), the corresponding HRP-conjugated secondary
126 antibodies (Invitrogen) and the SuperSignal West Pico PLUS kit (Thermoscientific).

127

128 **Genome sequencing and data analysis.** DNA was prepared from splenic amastigotes and
129 promastigotes at exponential culture phase. Parasites were centrifuged at 1,600 x *g* (pro) or 2,000 x *g*
130 (ama) for 10 min at room temperature. Approximately $1x10^8$ promastigotes from logarithmic growth
131 phase were re-suspended in 200 µl PBS and genomic DNA was purified using DNeasy Blood and
132 Tissue kit from Qiagen and RNase A according to the manufacturer's instructions. DNA concentrations
133 were measured in duplicate by fluorescence using a Molecular Device fluorescence plate reader (Quant-
134 IT kits, Thermo Fischer Scientific). The quality of DNA was controlled by determining the DNA
135 Integrity Number (DIN) analyzing 20 ng of DNA on a TapeStation 4200 (Agilent). One µg of genomic
136 DNA was used to prepare a library for whole genome sequencing on an automated platform, using the
137 Illumina "TruSeq DNA PCR-Free Library Preparation Kit", according to the manufacturer's
138 instructions. After normalization and quality control, qualified libraries were sequenced on a HiSeqX5
139 platform from Illumina (Illumina Inc., CA, USA) at the Centre National de Recherche en Génétique
140 Humaine (CEA, Evry, France), generating paired-ended, 150-bp reads. Sequence quality parameters
141 were assessed throughout the sequencing run. Standard bioinformatics analysis of sequencing data was
142 based on the Illumina pipeline to generate a FASTQ file for each sample.
143 Genomic DNA reads were aligned to the *L. donovani* Ld1S reference genome
144 (https://www.ncbi.nlm.nih.gov/bioproject/PRJNA396645, GCA_002243465.1) with BWA mem
145 (version 0.7.12) with the flag -M to mark shorter split hits as secondary. Samtools fixmate, sort, and
146 index (version 1.3) were used to process the alignment files and turn them into bam format (43).
147 RealignerTargetCreator and IndelRealigner from the GATK suite were run to homogenize indels (44).
148 Eventually, PCR and optical duplicates were labeled with Picard MarkDuplicates (version 1.94(1484))
149 (https://broadinstitute.github.io/picard/) using the option
150 "VALIDATION_STRINGENCY=LENIENT". For each read alignment file, Samtools view (version
151 1.3) and BEDTools genomecov (version 2.25.0) were used to measure the sequencing depth of each
152 nucleotide (45). Samtools was run with options "-q 50 -F 1028" to discard reads with a low map quality
153 score or potential duplicates, while BEDTools genomecov was run with options "-d -split" to compute
154 the coverage of each nucleotide. The coverage of each nucleotide was divided by the median genomic
155 coverage. This normalization is done to account for library size differences. The chromosome

156 sequencing coverage was used to evaluate aneuploidy between EP.1 and LP.1 samples. Then for each
157 sample and for each chromosome, the median sequencing coverage was computed for contiguous
158 windows of 2,500 bases. As previously published (46), the stably disomic chromosome 36 was used to
159 normalize chromosome read depth and to estimate chromosome polysomy levels in each sample. Gene
160 counts were produced using featureCounts (version 1.4.6-p3 (47)) with these parameters: -s 0 -t gene -
161 g gene_id and were normalized according to the median-ratio method.

162 For the generation of the chromosome median somy score heatmap, mean coverage in 300 bp bins as
163 generated by the GIP pipeline were used to compute somy scores per chromosome by first normalizing
164 bin scores for a sample by their median across all genome (to obtain comparable values between
165 samples), multiplying by two (to scale somy values to the default diploid state assumed for most of the
166 genome), and then taking the median across bins belonging to a given chromosome. These chromosome
167 scores were then displayed on a sample x chromosome heatmap, excluding the "maxi" chromosome.
168 This was done using the Pandas 1.4.2 {McKinney, 2010} (Reback *et. al*, 2021. Pandas-dev/pandas:
169 Pandas 1.2.4, https://zenodo.org/records/4681666)**,** Matplotlib 3.5.1 {Hunter, 2007} and Seaborn
170 0.11.2 {Waskom, 2021} Python libraries.

171 For the assessment of gene coverage ratio, normalized mean coverages per gene are reported
172 by GIP (version 1.1.0 (48)), as the mean coverage of the gene divided by the median coverage of the
173 chromosome containing the gene. For a given gene, and a given amastigote - promastigote pair, a gene
174 coverage ratio was computed adding 0.1 to the gene coverages of the individual samples, in order to
175 avoid zero division errors. The genes were sorted by genomic coordinate and assigned successive
176 integers to create a "genomic index". Gene coverage ratios were then plotted along this genomic index,
177 using the same Python libraries as above.

178 For the SNP analysis, alternative (Alt) allele frequencies for SNPs were retrieved from the
179 output of the SNV giptools module (provided along with the GIP pipeline). Euclidean distances between
180 samples in the SNP allele frequencies space were computed and used to build a dendrogram using the

181 scipy.cluster.hierarchy Python module (SciPy version: 1.8.0). The clustering was obtained using the
182 UPGMA method.
183
184 **RNA-seq analysis.** Total RNA was extracted from splenic amastigotes and promastigotes in
185 exponential culture phase. Amastigotes and promastigotes were centrifuged respectively at 2,000 x *g* or
186 1,600 x *g* for 10 min at 4°C, and re-suspended in the lysis buffer supplied with the Qiagen RNeasy Plus
187 kit. The samples were stored at -80°C and RNA extractions were performed according to the
188 manufacturer's instructions, including a DNase treatment. RNA integrity was controlled using the
189 Agilent Bioanalyzer. DNase-treated RNA extracts were used for library preparation using the TruSeq
190 Stranded mRNA sample preparation kit (Illumina, San Diego, California) according to the
191 manufacturer's instructions. An initial poly (A+) RNA isolation step (included in the Illumina protocol)
192 was performed on total RNA to remove ribosomal RNA. Fragmentation was performed on the enriched
193 fraction by divalent ions at high temperature. The fragmented RNA samples were randomly primed for
194 reverse transcription followed by second-strand synthesis to create double-stranded cDNA fragments.
195 No end repair step was necessary. An adenine was added to the 3'-end and specific Illumina adapters
196 were ligated. Ligation products were submitted to PCR amplification. The obtained oriented libraries
197 were controlled by Bioanalyzer DNA1000 Chips (Agilent, # 5067-1504) and quantified by
198 spectrofluorimetry (Quant-iT High-Sensitivity DNA Assay Kit, #Q33120, Invitrogen). Sequencing was
199 performed on the Illumina Hiseq2500 platform at the Biomics Center (Institut Pasteur, Paris, France)
200 to generate single-ended, 130-bp reads bearing strand specificity.
201 The bioinformatics analysis was performed using the RNA-seq pipeline 'Sequana' (49). Reads
202 were cleaned of adapter sequences and low-quality sequences using cutadapt (version 1.11) (50). Only
203 sequences of at least 25 nucleotides in length were considered for further analysis. STAR (version
204 2.5.0a) (51), with default parameters, was used for alignment on the reference genome
205 (GCA_002243465.1). Genes were counted using featureCounts (version 1.4.6-p3) (47) from Subreads
206 package (parameters: -t gene -g gene_id -s 1). Count data were analyzed using R version 3.6.1 (52) and
207 the Bioconductor package DESeq2 (version 1.24.0) (53). The normalization and dispersion estimation
208 were performed with DESeq2 using the default parameters and statistical tests for differential

209 expression were performed applying the independent filtering algorithm. For each pairwise comparison,
210 raw p-values were adjusted for multiple testing according to the Benjamini and Hochberg (BH)
211 procedure (54) and genes with an adjusted p-value lower than 0.01 were considered differentially
212 expressed.
213
214 **Label-free, quantitative total proteome analyses.** Untreated amastigotes (ama and ama-18h) and
215 promastigotes (pro), and lactacystin-treated parasites (ama lacta and pro lacta) were recovered and
216 washed three times with cold PBS at 2,000 x *g* or 1,600 x *g* for 10 min at 4°C. Parasite lysates were
217 prepared in eFASP lysis buffer (4% SDS / 0,2 % DCA / 50mM TCEP / 50 mM ammonium bicarbonate
218 buffer pH 8) (55). For detailed protocol see supplementary data file. MS scans were acquired at a
219 resolution of 70,000 and MS/MS scans (fixed first mass 100 m/z) at a resolution of 17,500. The AGC
220 target and maximum injection time for the survey scans and the MS/MS scans were set to 3 x 10^6 for
221 20 ms and 10^6 for 60 ms, respectively. An automatic selection of the 10 most intense precursor ions was
222 activated (Top 10) with a 40 s dynamic exclusion. The isolation window was set to 1.6 m/z and
223 normalized collision energy fixed to 28 for HCD fragmentation. We used a minimum AGC target of
224 10^4 corresponding to an intensity threshold of 1.7 x 10^5. Unassigned precursor ion charge states as well
225 as 1, 7, 8 and >8 charged states were rejected and peptide match was disable.
226
227 **Label-free quantitative phosphoproteome analyses.** Amastigote (ama) and promastigote (pro)
228 parasites were recovered and washed three times by centrifugation in cold M199 at respectively 2,000
229 x *g* or 1,600 x *g* for 10 min at 4°C. Samples were incubated for 10 min at 4°C in lysis buffer (1ml per
230 1.5x10^9 parasites) consisting of 8 M urea, 50 mM Tris, supplemented with a protease inhibitor cocktail
231 (cOmplete from Roche) and a phosphatase inhibitor cocktail (PhosStop from Roche). Following
232 sonication for 5 min using a sequence of 10 s pulse and 20 s pause, the lysates were centrifuged 15 min
233 at 14,000 x *g* and 4°C, and the supernatant was collected and stored at -80°C until use. Proteins were
234 quantified by RC DC protein assay (Bio-Rad) and adjusted to 1.3 $\mu g.\mu l^{-1}$ in lysis buffer. For detailed
235 protocol see supplementary data file. Phosphopeptide enrichment was carried out as described in (56)
236 and detailed in supplementary data. All analyses were performed on a Q Exactive HF Mass

237 Spectrometer (Thermo Fisher Scientific) coupled with a Proxeon EASY-nLC 1000 (Thermo Fisher
238 Scientific) as detailed in supplementary data. Details for the proteomics and phosphoproteomics
239 analyses following the data acquisition are available in supplementary data. Results are presented in
240 table 6 and 10.

241 Phosphopeptides were selected for Gene Ontology enrichment analyses if (i) they were
242 exclusively identified in one of the two stages, (ii) they showed significant, stage-specific changes in
243 phosphopeptide abundance (fold change ≥ 2, adj. p-value < 0.01) even if the corresponding protein was
244 not detected in the total proteome analysis, and (iii) they showed a significant increase in
245 phosphostochiometry (p-value < 0.05) as calculated by the ratio 'change in phosphopeptide abundance'
246 vs 'change in protein abundance' using a cut off of fold changes ≥ 2 and adj. p-value < 0.01 for both
247 analyses (see table 11).

248

249 **Metabolomic analysis.** The sample extraction was performed as described previously (57). Briefly, 10^8
250 cells were used per each 200 µL sample. Firstly, cells were rapidly quenched in a dry ice/ethanol bath
251 to 4°C, then centrifuged, washed with 1 x PBS, and resuspended in the extraction solvent
252 (chloroform:methanol:water, 1:3:1). After vigorous shaking at 4°C for 1 h, extracts were centrifuged
253 (16,000 x g, 4°C, 10 min) and the supernatants collected and stored at -80°C until the analysis. LC-MS
254 analyses were performed using separation on 150 x 4.6 mm, 5 mm ZIC-pHILIC (Merck) on UltiMate
255 3000 RSLC (Thermo Scientific) followed by mass detection on an Orbitrap Exactive mass spectrometer
256 (Thermo Fisher) at Glasgow Polyomics. Analyses were performed in positive and negative polarity
257 switching mode, using 10 µl injection volume and a flow rate of 300 µl/min over 26 min on the column
258 maintained at 30ºC, as follows: 0 to 20 min 20%-to 80% solution A, 15 to 17 min 95% solution A, 17
259 to 26 min 20% solution A where solution A is 20 mM ammonium carbonate in water and solution B is
260 acetonitrile). The samples were run alongside 249 authentic standards at 10 µM each. Mass
261 spectrometry data was processed using Mzmatch (58) and Ideom (57) software. Unique signals were
262 extracted using the centwave algorithm and matched across biological replicates based on mass-to-
263 charge ratio and retention time. These grouped peaks were then filtered based on relative standard
264 deviation and combined into a single file. The combined sets were then filtered on signal-to-noise score,

265 minimum intensity and minimum detections. The final peak set was then gap-filled and converted to
266 text for use Putative metabolite identification corresponds for the most part to Metabolite Standards
267 Initiative (MSI) level 2 (mass only, and thus only considered a tentative annotation), whereas
268 metabolites matching in retention time to an included standard correspond to level 1 (considered likely
269 an accurate annotation). Peaks having an area with root squared deviation across pooled samples > 50%
270 were excluded, as were those with a retention time < 4 min (due to poor resolution).
271
272 **Quantification of pre-snoRNA levels.** DeSeq2 analysis was performed on two biological replicates of
273 amastigote and promastigote poly(A)-RNA libraries prepared as previously described (34). Fold change
274 > 1.5 and adj. p-value < 0.05 was considered as significantly upregulated RNA and Fold change <1.5,
275 adj. p-value < 0.05 was considered as significantly downregulated RNA.
276
277 **Localizing rRNA modification on Leishmania cryo-EM ribosome structure**. The cryo-EM atomic
278 model of *Leishmania major* 80S ribosomes bound to mRNA and all three tRNAs (PDB: 8RXH) was
279 used to indicate rRNA modifications of the ribosome. Figures were generated using UCSF Chimera-X
280 software (59).
281
282 **Systems-level analyses.** A lists of *L. donovani* GO terms (60) was built in house. The Biological
283 Networks Gene Ontology tool (BiNGO) plugin of the Cytoscape software package (version 3.8.2) was
284 used to map and visualize functional enrichments in each data set based on the GO hierarchy. A
285 Benjamini & Hochberg false discovery rate with a significance level of 0.05 was applied. Cluster
286 efficiency represents the percentage of genes for a given GO term compared to the total number of
287 genes with any GO annotation in the considered set of genes. Enrichment score corresponds to the
288 percentage of genes for a given GO term compared to all the genes sharing the same GO term in the
289 genome. Word Cloud of GO enrichment analysis limited to GO Slim terms and a threshold of p-value
290 < 0.05 for the category Biological Process was performed on TriTrypdb (https://tritrypdb.org) using the
291 *L. donovani* LdBPK orthologs for all genes that showed statistically significant expression changes (p-
292 value < 0.01) at both RNA or protein levels.

293 For the phosphoproteomic work, phosphopeptides were selected for Gene Ontology enrichment
294 analyses if (i) they were exclusively identified in one of the two stages, (ii) they showed significant,
295 stage-specific changes in phosphopeptide abundance (fold change ≥ 2, adj. p-value < 0.01) even if the
296 corresponding protein was not detected in the total proteome analysis, and (iii) they showed a significant
297 increase in phosphostochiometry (p-value < 0.05) as calculated by the ratio 'change in phosphopeptide
298 abundance' vs 'change in protein abundance' using a cut off of fold changes ≥ 2 and adj. p-value < 0.01
299 for both analyses (see table 11). Functional enrichment networks were built with the STRING plugin
300 of the Cytoscape software package (version 3.8.2) using the *L. infantum* orthologs and a Benjamini &
301 Hochberg p-value threshold < 0.05. The "ClusterProfiler" package (version 4.2.2) of R was used for
302 KEGG (Kyoto encyclopedia of genes and genomes) gene set enrichment analysis (GSEA) and for data
303 mapping on metabolic pathways available in the KEGG database. Results were visualized using the
304 "pathview" packages (version 1.34.0).
305
306 **Data availability.** The mass spectrometry proteomics data were deposited to the ProteomeXchange
307 Consortium via the PRIDE partner repository with the dataset identifiers PXD035697
308 (phosphoproteome data) and PXD035698 (proteome upon lactacystin treatment) (61). The DNAseq
309 data have been deposited in NCBI's Gene Expression Omnibus (62) PRJNA1231373 and are
310 accessible in the BioProject PRJNA1231373 (https://www.ncbi.nlm.nih.gov/sra/PRJNA1231373).
311 The RNAseq data have been deposited in NCBI's Gene Expression Omnibus (62) and are accessible
312 through GEO Series accession number GSE227637
313 (https://www.ncbi.nlm.nih.gov/geo/query/acc.cgi?acc= GSE227637). The mass spectrometry
314 metabolomic data were deposited in the Metabolights data repository.
315
316
317 **RESULTS**
318 ***Leishmania* stage differentiation occurs independently from changes in gene dosage.** We carried
319 out an in-depth, systems analysis of independent *L. donovani* amastigote preparations isolated from
320 infected hamster spleens and their culture-derived promastigotes at *in vitro* passage 2, with the aim of

321 revealing mechanisms controlling stage-specific differential expression across five quantifiable
322 information levels, by comparing the genome, transcriptome, proteome, metabolome and phospho-
323 proteome of the two life-cycle stages (Figure 1A and Figure S1). We first investigated the possible role
324 of genome instability in stage-differentiation, given the very well documented propensity of *L. donovani*
325 to establish and tolerate chromosome and gene copy number variations in culture and during sand fly
326 or hamster infection (46, 60, 63).

327 Applying our computational pipeline termed 'GIP' (48) to the genome sequences of three
328 independent pairs of amastigotes and promastigotes confirmed the largely disomic state of the
329 *Leishmania* genome at both stages, except for the known constitutive tetrasomy of chr 31 (Figure 1B
330 and Figure S2A, Table 1). While we did not detect any major changes at karyotypic levels, a clear
331 pattern emerged for promastigotes that showed a slight but reproducible increase in median coverage
332 for chr 1, 2, 3, 4, 6 and 20, suggesting the emergence of mosaic aneuploidy for these chromosomes
333 early during culture adaptation. Likewise, stage differentiation was not associated with any major gene
334 copy number variation (Figure 1C, Table 2). Even though a number of genes showed increased (e.g.
335 Ld1S_300477100 encoding an intraflagellar transport (IFT) protein) or decreased (e.g.
336 Ld1S_220235700 encoding a hypothetical protein) read depth in individual pro strains, none of these
337 changes converged across all pro samples, suggesting that they may either represent intrinsic variations
338 between different amastigote isolates or are the result of random genetic drift, likely caused by the bottle
339 neck effect represented by culture inoculation. Plotting the normalized read depth ratios between
340 amastigotes and promastigotes revealed an intriguing, undulating pattern that was highly reproducible
341 across the three independent experiments and has been previously associated with nascent DNA
342 produced during the replicative S-phase of the cell cycle (64-66). Finally, differentiation did not affect
343 the SNP frequency distribution (Figure S2B, Table 3), which resulted in a largely diagonal pattern when
344 plotting amastigote against promastigote SNP frequencies (Figure 1D).

345 In conclusion, in contrast to fitness gain (46, 67), *L. donovani* promastigote differentiation *in*
346 *vitro* is independent of genomic adaptation, confirming our previous results obtained with sand fly-
347 derived parasites (60, 68).

348

349 **Comparative RNA-seq analysis reveals stage-specific regulons that are controlled at post-**
350 **transcriptional levels.** We next analyzed stage-specific expression changes applying RNA-seq
351 analyses on two amastigote and derived promastigote strains. In contrast to the relatively stable genome
352 infrastructure maintained between stages, we observed substantial, stage-specific differences in
353 transcript abundance. From 8850 detected transcripts in both stages, 4998 showed statistically
354 significant differences (adj. p-value < 0.01), including 531 and 1082 transcripts with a 2-fold or higher
355 increase in abundance in amastigotes and promastigotes, respectively (Figures 2B left panel,) (Table 4).
356 Considering the lack of promoter-driven control of gene expression in *Leishmania* and the absence of
357 stage-specific gene dosage effects (see Figure 1), the observed differences in amastigote and
358 promastigote transcript abundances are most likely attributable to stage-specific mRNA turnover.
359 Direct comparison of replicate transcriptomes did not identify any significant differences between the
360 two independent amastigote and promastigote expression profiles, revealing the high fidelity of post-
361 transcriptional mechanisms that govern stage-specific mRNA turnover (Figure 2A).
362 Analyzing the stage-specific RNA-seq data sets identified clusters of co-regulated transcripts
363 that share a common annotation, which therefore define distinct regulons (Figure 2B, Table 4). In
364 amastigotes, one major positive regulon showing increased abundance included 83 amastin transcripts
365 encoded on 5 different chromosomes, confirming the post-transcriptional co-regulation of this gene
366 family as previously described (19, 69, 70) (Table 4, sheet C and E). Another positive regulon in
367 amastigotes was associated with protein translation, with GO enrichment observed for the terms
368 'ribosome biogenesis' (38 transcripts), 'rRNA processing' (27 transcripts), 'tRNA processing' (7
369 transcripts), or 'RNA methylation' (5 transcripts) (Figure 2B, middle panel). These data reveal the
370 ribosome and epi-transcriptomic regulation as possible central components in *Leishmania* stage
371 differentiation.
372 In promastigotes, a first positive regulon included 23 transcripts annotated for the GO term
373 'ciliary cell motility', confirming the post-transcriptional co-regulation of flagellar biosynthesis as
374 previously shown in *L. mexicana* (71) (Figure 2B right panel, Table 4, sheet F). Further regulons are
375 defined by the GO terms 'oxidative phosphorylation' (12 transcripts), 'oxidation reduction' (46
376 transcripts), and 'translational elongation' (28 transcripts), the latter suggesting translational control as

377 a further regulatory step in stage differentiation. Finally, the largest promastigote-specific regulon is
378 represented by 53 transcripts annotated for 'post-transcriptional regulation of gene expression'.
379 In conclusion, our RNAseq data reveal a series of stage-specific regulons whose mRNA
380 stability is regulated in a coordinated manner. Whether this co-regulation is governed by stage-specific
381 mRNA decay mechanisms acting on 5' and 3' UTRs or by stage-specific mRNA stabilization via RNA-
382 binding proteins or mRNA modification remains to be established.
383
384 **Quantitative proteome analysis reveals regulons that are independent of stage-specific**
385 **mRNA turnover.** We next employed quantitative proteomic analysis to assess how the different
386 regulons observed in our RNAseq analyses translate into stage-specific proteomes. Label-free
387 quantitative proteomic analysis of 4 independent biological replicates of amastigotes and derived
388 promastigotes identified over 4000 proteins at each stage in at least 3 out of 4 biological replicates,
389 representing 3521 differentially expressed proteins (adjusted p-value < 0.01), 1534 of which were
390 exclusively detected in either ama or pro (Figure 3A left panel, Table 6). Considering the 822 proteins
391 that are specific or more abundant in amastigotes (fold change ≥ 2), functional enrichment was mainly
392 observed for the GO terms 'oxidation reduction' (61 proteins), 'vesicle mediated transport' (23 proteins)
393 and 'phosphorylation' (41 proteins) (Figure 3A, middle panel, Table 6, sheets B and D). Considering
394 the 1637 proteins that are specific or more abundant in promastigotes (fold change ≥ 2), functional
395 enrichment was observed for the GO terms 'post-transcriptional regulation of gene expression' (71),
396 'translation' (69 proteins), 'ribosome biogenesis' (21 proteins) and 'ciliary cell motility' (42 proteins)
397 (Figure 3A, right panel, Table 6, sheet C and E). The metabolomic analysis of four independent
398 amastigote and promastigote samples (Figure S4A) support our proteomic data. Promastigotes showed
399 increased amino acid biosynthetic activity that matched the changes in protein abundance observed for
400 this pathway, while the amastigote metabolome indicates a shift from glycolytic to TCA cycle-
401 dependent energy production that was previously described (12, 14, 72) (Figures S4B-D), with a notable
402 increase in metabolites involved in butanoate metabolism indicative of a shift between carbohydrate
403 use as a primary energy source to utilization of fatty acid oxidation. While succinate and malate levels
404 were diminished this is because these metabolites comprise a glycosomal succinate shunt related to

405 glycolysis in addition to their roles in the TCA cycle. The amastigote expression profile and
406 metabolome further indicate the stage-specific production of the storage-carbohydrate mannogen, thus
407 confirming previous observations (73) (Figure S4E). Surprisingly, only few enriched GO terms
408 correlated between transcriptomics and proteomics datasets, suggesting additional layers of regulation
409 between the transcriptional and translational levels of gene expression. To investigate this aspect on a
410 genome-wide level, we next plotted the simple numerical values we obtained when calculating the ratios
411 of expression changes between ama and pro observed in the transcriptomics and proteomics datasets
412 (Figure 3B, Table 7). The double ratio analysis of 2076 genes showing statistically significant
413 expression changes at both mRNA and protein levels (p-value < 0.01) defined four quadrants:
414 Quadrants 2 (Q2) and 4 (Q4) correspond to 365 and 918 genes (Table 7, sheet E and I), respectively,
415 for which stage-specific expression changes correlate between protein and RNA levels, suggesting that
416 the abundance of these proteins is mainly regulated by mRNA turn-over. Q2 (mRNA and protein up in
417 ama) includes the GO terms 'vesicle mediated transport' (14 genes) and 'lipid metabolic process' (18
418 genes) (Table 7, sheet F), while Q4 (mRNA and protein up in pro) includes the GO term 'cell motility'
419 (41 genes) (Table 7, sheet J).

420 Counter-correlations between RNA and protein abundances (p-value < 0.01) were observed for
421 381 and 412 genes, respectively falling into quadrants Q1 (RNA down and protein up in ama) and Q3
422 (RNA down and protein up in pro) (Figure 3B, Table 7, sheets C and G). The most important difference
423 was observed for 38 genes annotated for the GO term 'ribosome biogenesis' (Figure 3C, Table 7, sheet
424 H). While this GO term defined a positive regulon at mRNA level in amastigotes (see Figure 2B), the
425 same genes show reduced expression at this stage at protein level (Figure 3C). This lack of correlation
426 may be explained by stage-specific changes in mRNA translation efficiency. While it was technically
427 impossible to enrich enough material from spleen-derived amastigotes to perform in-depth ribo-
428 profiling analyses, we obtained indirect evidence for differential translational control: First, analyzing
429 poly-A transcriptome libraries of amastigotes and promastigotes we observed significant differences in
430 stage-specific expression of 110 pre-snoRNAs (Table 5, Figure 3D). These data fit with the GO
431 enrichment 'ribosome biogenesis' observed in the promastigote proteome and the expression of a series
432 of methyl- and pseudouridyl-transferases at this stage (see Table 6, sheets A and E). Second, by

433 localizing RNA modification on high resolution cryo-EM structure of *Leishmania* ribosome we indeed
434 observed important stage-specific changes in Pseudouridine and 2'-O-Methylation rRNA modifications
435 (Figure 3 E), which are known to affect the ribosome translational activity (34).
436 In conclusion, the discrepancies observed between transcript and protein abundances in *L.*
437 *donovani* amastigotes and promastigotes reveals stage-specific regulatory mechanisms independent of
438 mRNA stability, which may act at the level of translational control, or rely on differential protein
439 stability as investigated below.
440
441 **Stage-specific protein turn-over is required for parasite differentiation.** The poor correlation we
442 observed between changes in mRNA and protein abundance during the amastigote-to-promastigote
443 transition (see Figure 3B) primed us to investigate the role of proteasomal protein degradation in
444 *Leishmania* differentiation by employing the highly specific and irreversible proteasome inhibitor
445 lactacystin (74). Comparative, quantitative proteomics analyses were performed with (i) spleen-derived
446 amastigotes (ama), (ii) amastigotes after the first 18h of differentiation in the absence (control, ama-
447 18h) and the presence of latacystin (ama-lacta), and (iii) promastigotes in culture without (pro) and after
448 18h of treatment with lactacystin (pro-lacta) (Table 8, Figure 4A and S5).
449 First, this data set allowed us important insight into processes of early differentiation, revealing
450 increased abundance in ama-18h compared to ama for 694 proteins (fold change ≥ 2, adjusted p-value
451 < 0.01) (Table 8b, sheet B) with GO enrichment observed for the terms 'ribosome biogenesis', 'RNA
452 methylation', 'rRNA processing', 'gene expression', and 'post-transcriptional regulation of gene
453 expression', the latter including 6 genes encoding for pseudouridine transferases known to modify
454 ribosomal (r) RNA (Figures S5A and S6) (Table 8b, sheets D to H). These data further sustain a role of
455 epitranscriptomic regulation and stage-adapted ribosomes as key processes that may initiate *Leishmania*
456 promastigote differentiation, at least in culture.
457 Second, lactacystin treatment uncovered an essential regulatory role of proteasomal protein
458 degradation in *L. donovani* development. While the presence of the inhibitor neither affected parasite
459 viability (Figure S7A) nor promastigote growth (data not shown), lactacystin treatment abrogated the
460 amastigote-to-promastigote developmental transition as judged by the persistence of an amastigote-like

461 morphology (i.e. oval cell shape, retracted flagellum), and the absence of PFR2 expression
462 characteristic of promastigotes (Figures 4B and C). In contrast, untreated amastigotes spontaneously
463 converted to flagellate promastigotes after 48h in culture (Figure S7B and C).

464 Finally, comparing the proteomics signatures of lactacystin-treated samples and untreated
465 controls (Figure S5) allowed us to reveal the proteasomal targets, whose rescue correlated with the
466 observed abrogation of differentiation. This analysis is complicated by the fact that amastigotes will not
467 only respond to the 18h treatment but also initiate their differentiation into promastigotes during this
468 period. To distinguish changes caused by lactacysin treatment from changes due to the differentiation,
469 we plotted the ratio of ama/ama-lacta against the ratio ama-18h/ama-lacta (Figure 4D), which defined
470 one quadrant (Q3) representing 129 proteins whose increased abundance in ama-lacta was exclusively
471 due to rescue from degradation (Table 9, sheet A). Applying STRING and GO analyses on these
472 proteins revealed enrichment for the terms 'protein kinase', 'cellular response to stimulus', and 'cell
473 cycle' (Figure S8 lower panel, Table 9, sheet B and G).

474 Proteomics analysis of lactacystin-treated promastigotes (pro-lacta) revealed the rescue of 289
475 proteins from degradation when compared to untreated control (pro) (Table 9, sheet C). Comparison of
476 rescued proteins across both ama and pro stages revealed a series of intriguing findings: First, most of
477 these proteins were rescued in a stage-specific manner, confirming differential protein degradation as
478 an important new regulatory component in the development and maintenance of *Leishmania* life cycle
479 stages as suggested by previous reports (37, 75-81). Second, just like the proteins rescued from
480 proteasomal degradation in ama-lacta, the pro-lacta data set too showed GO enrichment for the terms
481 'protein kinase' and 'cellular response to stimulus', involving distinct sets of proteins (Figure S8, upper
482 panel) (Table 9, sheets D, E and G). Thus, rather than being controlled by a single master regulator,
483 *Leishmania* differentiation seems to be governed by complex signaling networks that are established in
484 a stage-specific manner involving proteasomal degradation. Third, when mapping the lactacystin-
485 rescued proteins to the established, stage-specific proteomes (Figure 4E), an intriguing pattern emerged:
486 the majority of proteins that were rescued in ama-lacta turned out to be expressed specifically in the
487 promastigote proteome. *Vice versa,* many proteins rescued in pro-lacta were part of the amastigote-
488 specific proteome (Table 9, sheets H and I), a pattern that affected 14 protein kinases (Figure 4F). Thus,

489 these proteins are expressed constitutively across both stages, while their steady-state stage-specific
490 abundance is regulated by proteasomal degradation. Surprisingly, 12 proteins (including the protein
491 kinase Ld1S_220237000) were rescued from degradation in both ama-lacta and pro-lacta but were
492 never identified in the proteomes of the corresponding untreated controls, suggesting that they are
493 constitutively degraded in both stages under our experimental conditions (Figure 4G, Table 9, sheet F).
494 In conclusion, our results reveal an unexpected but substantial role of protein degradation in
495 regulating the *L. donovani* amastigote and promastigote proteomes and identify protein kinases as key
496 targets of stage-specific proteasomal activities.
497
498 **Quantitative phosphoproteome analysis reveals *Leishmania* reciprocal and recursive regulatory**
499 **networks underlying stage differentiation.** The investigations above associated the expression of
500 protein kinases (and their degradation) to *Leishmania* stage differentiation (Figure 4F, S8 and S9), thus
501 confirming previous reports on the importance of phosphotransferase activities in trypanosomatid
502 development (82-92). Differential turnover of these important signaling proteins by stage-specific
503 proteasomal activities likely represents a regulatory switch controlling parasite development. To further
504 investigate how this putative regulatory switch operates, we screened for stage-specific protein kinase
505 substrates applying label-free, quantitative phospho-proteomic analyses on three independent
506 amastigote and promastigote samples. We identified a total of 2079 phospho-peptides in amastigotes
507 and 7095 phospho-peptides in promastigotes, suggesting a three-fold increase in global protein
508 phosphorylation in insect-stage parasites (Table 10). However, increased TiO_2 phosphopeptide
509 enrichment in a given sample may be due either to increased substrate expression or increased *de novo*
510 phosphorylation (Figure 5A and S10). To distinguish between these two possibilities and assess the
511 stage-specific phospho-stoichiometry, we normalized changes in protein phosphorylation against
512 changes in protein abundance (Figure 5B).
513 We identified 877 phosphoproteins in amastigote samples carrying 2079 phosphosites of which
514 55.8% (1160) were uniquely identified at this stage, while 12.6% (565) showed a significant change in
515 phospho-stoichiometry compared to promastigotes (Figure S10, Table 11 sheets A to D). Conversely,
516 2054 phosphoproteins with 7095 phosphorylation sites were identified in promastigote samples, of

517 which 70% (4967) were exclusively detected at this stage, while 1% (73) presented a significant change
518 in phospho-stoichiometry compared to amastigotes (Figure S10, Table 11 sheets F to I). These data
519 reveal a surprising level of stage-specific phosphorylation in promastigotes, which may reflect their
520 increased biosynthetic and proliferative activities compared to amastigotes.

521 We next investigated the pathways regulated by phosphotransferase activities analyzing the
522 phosphoproteomes of amastigote and promastigote for enriched biological processes (Figure 5C) (Table
523 11, sheets E and J). Stage-specific enrichment was observed in the pro dataset for 'ciliary cell motility',
524 indicating that flagellar biogenesis and activity are not only regulated by increased protein abundance,
525 but also by increased phospho-stoichiometry of flagellar proteins. Surprisingly, similar functions were
526 enriched in both the differential datasets linked to cell division (e.g. 'cytokinesis', 'cell cycle'),
527 signaling (e.g. 'protein aa phosphorylation', 'signal transduction'), or post-transcriptional regulation of
528 gene expression. Thus, aside stage-specific protein turnover (see above, Figure 4), differential
529 phosphorylation represents yet another layer of regulation that contributes to the establishment of stage-
530 specific biological networks in *Leishmania*.

531 Analyzing stage-enriched, functional networks in further detail using the STRING applications
532 of the Cytoscape software package revealed a series of intriguing regulatory interactions (Figure S11,
533 Table 12): First, a group of protein kinase substrates are protein kinases themselves with more than 30
534 and 100 members of this large protein family identified in the ama and pro phosphoproteomes,
535 respectively (Table 11, sheets D and H, see Figure 5D for phosphorylation pattern of some members of
536 the MAP kinase pathway). Second, both amastigote and promastigote phosphoproteomes include stage-
537 specific phosphatases (18 in ama and 55 in pro) that can counteract protein kinase activities and even
538 deactivate signaling cascades by dephosphorylation of protein kinase substrates (Figure S11, Table 11,
539 sheets D and H). Furthermore, the stage-specific phosphoproteomes showed enrichment in functional
540 networks linked to ribosomal biogenesis and RNA processing suggesting that protein kinases may
541 control the establishment of stage-specific ribosomes. Finally, the identification of networks linked to
542 proteasomal protein degradation in both ama and pro datasets not only further sustains the role of protein
543 turnover in *Leishmania* stage differentiation, but uncovers a feedback loop with proteasomal activities
544 controlling stage-specific degradation of protein kinases (see Figure 4), which in turn control stage-

545 specific ubiquitin ligases and deubiquitinating enzymes (see Figure 5D for phosphorylation pattern of
546 selected members of the Ubiquitin proteasomal system).
547
548
549
550

551 **Discussion**

552 Applying a 5-layer molecular systems analysis on spleen-derived bona fide amastigotes and culture-
553 derived promastigotes, we uncovered a series of regulatory interactions during parasite stage
554 differentiation that act within and between the levels of transcript stability, translational regulation,
555 proteasomal protein turnover, and protein phosphorylation. Our data reveal an unexpected complexity
556 of the *Leishmania* developmental process and raise important questions on the type of regulatory
557 feedback loops that govern parasite stage differentiation, their biological integration, and their role in
558 adaptation and phenotypic robustness.

559 A first series of regulatory networks identified in our experimental system rely on recursive or
560 self-controlling interactions, where components of a given pathway are regulated by the pathway itself
561 (Figure 6A). In promastigotes for example, a large regulon showing stage-specific increase in transcript
562 abundance was defined by the GO term 'post-transcriptional regulation of gene expression'. In the
563 absence of any significant gene dosage changes between amastigotes and promastigotes, and given the
564 lack of transcriptional control in *Leishmania*, the differential expression of these transcripts itself must
565 be regulated at the post-transcriptional level, thus establishing a recursive feedback loop. Our data
566 uncovered a similar recursive feedback loop acting on the level of protein translation, which was
567 revealed by a paradox: while amastigotes showed increased abundance for 38 transcripts annotated for
568 the GO term 'ribosome biogenesis' (Table 4, sheet E), the corresponding proteins were of diminished
569 abundance in amastigotes compared with promastigotes (Figure 3C). This dissociation between RNA
570 and protein abundances indicates that ribosomal components themselves may be regulated at
571 translational levels. Increased ribosomal protein abundance in promastigotes likely satisfies the
572 requirement of increased translation capacity at this fast-growing stage (31, 93). In contrast, increased
573 mRNA abundance of ribosomal components in amastigotes may indicate stage-specific mechanisms of
574 mRNA storage (94) that may allow to jump start promastigote differentiation and accelerated growth
575 following exposure to low temperature and neutral pH. This possibility is directly supported by our
576 proteomics investigations, revealing ribosomal biogenesis as one of the first pathways induced over the
577 initial 18h during the amastigote-to-promastigote developmental transition.

578 Differentiation to promastigotes was associated not only with a quantitative change of
579 ribosomes as indicated by the upregulation of a variety of ribosomal proteins and translation factors
580 (see Table 8), but also with a qualitative change of likely ribosome structure as indicated by the enriched
581 GO terms 'RNA methylation' and 'pseudouridine synthesis' that respectively include genes encoding
582 for 8 methyltransferases (e.g. the rRNA methyltransferases Ld1S_350672300 and Ld1S_350694000),
583 6 pseudouridine synthases (Table 8, sheets D to H), and the H/ACA snoRNP Nop10
584 (Ld1S_360722900). The differential expression of snoRNAs (see Figure 3D and Table 5) and the
585 developmentally regulated changes in rRNA modification that can affect ribosome activity (34) (Figure
586 3E and C) suggest the existence of stage-specific ribosomes. This finding is in line with our recent
587 reports providing indication for specialized ribosomes in *Leishmania* adaptation, in which we correlated
588 changes in rRNA pseudouridylation to *L. donovani* fitness gain in culture (31, 60).

589 Finally, a third recursive feedback loop acted at the post-translational level involving members
590 of various protein kinase families, which not only showed stage-specific expression, but also
591 represented a main class of phosphorylation substrates themselves. This recursive interaction likely
592 reflects stage-specific signaling cascades, where downstream kinases are activated through
593 phosphorylation by upstream kinases, such as exemplified by the MAP kinase pathway (92, 95). Indeed,
594 11 members of the MAP kinase family showed stage-specific changes in their phosphorylation pattern
595 (Figure 5D), 9 of which were only detected in the promastigote phospho-proteome and were previously
596 associated with this stage, being implicated in flagellar biogenesis (MPK9 and MPK3) or
597 metacyclogenesis (MPK4) (87, 91, 96). In contrast, the two MAP kinases MPK2 and MPK10 -
598 previously linked to amastigote differentiation and virulence (88, 91) - showed an amastigote-specific
599 increase in protein abundance and phospho-stoichiometry for defined phosphorylation sites.

600 Protein kinases not only engage in recursive regulatory interactions but are also at the center of
601 a second form of feedback loop defined by reciprocal interactions, where components of two or more
602 regulatory pathways can cross-control each other (Figure 6A). Phospho-stoichiometry analysis places
603 protein kinases at the center of three such loops: First, stage-specific kinase activities act on a series of
604 phosphatases that in return can modify kinase activities by dephosphorylation (Table 11, sheets D and

605 G). Second, 47 proteins associated with 'Translation' were identified in the stage-specific phospho-
606 proteomes. Most of these proteins showed promastigote-specific phosphorylation, including 23
607 different ribosomal proteins and 15 eukaryotic translation initiation factors including eIF-2a, eIF-3
608 (subunits a, b, g, h), eIF-4A1, eIF-4G1-1, -2 and -5, or eIF-5a, of which many have been linked to
609 various *Leishmania* biological process, such as translational control, cell cycle regulation or infectivity
610 (29, 97-101). This opens the possibility of yet another reciprocal feedback loop, where phosphorylation
611 of ribosomal components fine tunes translational control, which in turn may affect the expression of
612 protein kinases themselves (102-110).

613 Finally, our results revealed a third reciprocal feedback loop between protein kinases and
614 proteins linked to the proteasomal system. 11 ubiquitin hydrolases (also known as deubiquitinases,
615 DUBs) and 10 ubiquitin ligases/transferases showed stage-specific phosphorylation at specific residues
616 (Table 11, sheets D and I), while 14 protein kinases underwent differential proteasomal degradation
617 (Figure 4F, Table 9, sheet G). These included two protein kinases that have previously been linked to
618 *Leishmania in vivo* fitness (91), RDK1 (Repressor of differentiation kinase 1, Ld1S_320540600) and
619 DIK (differentiation inhibitory kinase, Ld1S_280397500), whose rescue from degradation correlated
620 with stalled amastigote-to-promastigote transition. Surprisingly, 5 protein kinases showed constitutive
621 degradation across both stages. The constitutive expression of many proteasomal components across
622 both amastigote and promastigote stages further supports a role of phosphorylation in regulating the
623 observed, stage-specific proteasomal activities, considering that phosphorylation of DUBs has been
624 linked to changes in their stability, localization, specificity or catabolic activity (111, 112).

625 Several arguments support a central role of this kinase/proteasome reciprocal feedback loop in
626 early parasite development. First, proteasomal activities are known to allow for rapid proteome
627 remodeling during trypanosomatid differentiation (81, 113, 114). Second, *Leishmania* stage
628 differentiation is triggered by environmental pH and temperature changes, which can be sensed and
629 translated into biological information by MAP kinase signaling cascades (84, 115). Finally, our data
630 reveal a direct and essential role of this reciprocal regulation in the *Leishmania* amastigote-to-
631 promastigote transition, which was abrogated in the presence of the proteasomal inhibitor lactacystin.
632 This observation is reminiscent of previous reports genetically validating an essential role for the *L.*

633 *mexicana* ubiquitin conjugating (E2) enzymes UBC1/CDC34, UBC2 and UEV1, and the HECT E3
634 ubiquitin ligase HECT2 in promastigote to amastigote differentiation (81). Likewise, proteasomal
635 activities were implicated in *T. cruzi* proliferation and differentiation (113, 116-118). The complexity
636 of regulatory interactions between protein kinases and the proteasomal pathway is further increased by
637 observations showing that substrate phosphorylation can mediate subsequent ubiquitination and
638 degradation, while ubiquitination of MAP kinase family members can regulate kinase activity and
639 localization rather than promote degradation (119-121). Future experiments simultaneously analyzing
640 changes in both phosphoproteome and ubiquitome during *Leishmania* stage-differentiation may help
641 elucidate this complex regulatory interaction and identify individual proteins and their PTMs that drive
642 parasite development.

643 In conclusion, our data allow unprecedented insight into the regulatory landscape of
644 *Leishmania* stage development. We reveal genetic feedback control as a central mechanism in parasite
645 differentiation, with stage-specific interactions between genes and their products adapting the parasite
646 phenotype to the environmental changes encountered inside its vertebrate and invertebrate hosts. In
647 contrast to the major phenotypic shift observed between mammalian-stage amastigotes and insect-stage
648 promastigotes, each developmental stage is stably maintained within its respective host even in the wake
649 of environmental fluctuations. Such phenotypic robustness is known to rely on highly inter-connected,
650 stage-specific regulatory networks (122), which in the case of *Leishmania* implicates recursive and
651 reciprocal genetic interactions between protein translation, protein degradation and protein
652 phosphorylation (Figure 6B and C). *Leishmania* differentiation thus represents an excellent model
653 system to study how alternations between phenotypic plasticity (i.e. developmental transitions) and
654 robustness (stable maintenance of stages) shape microbial fitness and allow for the emergence of
655 adaptive biological traits. However, despite the robustness of a given stage, we previously showed that
656 *Leishmania* still can fine-tune adaptive phenotypes in a given stage to promote fitness via interactions
657 between gene dosage changes and compensatory responses at the post-transcriptional and translational
658 levels (31, 60). This insight bears important consequences for future studies on *Leishmania* adaptation
659 in clinical settings, which should combine multi-layer systems analyses such as described here with

660 deep learning algorithms that allow for data integration and the identification of novel biomarkers on
661 phenotypic and homeostatic rather than genetic levels.

662

663

664

665 **Figure legends**

666

667 **Figure 1: Comparative genomic analysis of *L. donovani* lesion-isolated amastigotes and derived**
668 **promastigotes.** (A) Schematic overview of the parasite samples used for the various systems level
669 analyses presented in this study. A more detailed overview is shown in Figure S1. (B - D) Genomic
670 analyses. (B) Heatmap showing the somy score of three individual differentiation experiments using
671 hamster-isolated amastigotes (ama1, ama2 and ama3) and their corresponding, culture-derived
672 promastigotes analysed at passage 2 (pro1, pro2 and pro3). Samples and chromosomes are indicated on
673 the x- and y-axis, respectively. The somy scores were calculated as described in Material and Methods
674 and correlate to the grey level according to the shown legend. (C) Ratio plot showing the gene coverage
675 ratio ama versus pro (y-axis) for all genes across the 36 chromosomes (x-axis) as calculated based on
676 normalized median read depth. Each color represents one individual differentiation experiment using
677 ama isolates from individual hamsters. The red dotted lines indicate the ratio values corresponding to
678 1.5 (upper line) and 0.5 (lower line), indicating respectively gain or loss of one gene copy in the ama
679 samples. (D) Correlation plots representing the individual (histograms on the diagonal) and pairwise
680 (off-diagonal scatterplots) distributions of SNP frequencies for the indicated samples.

681

682 **Figure 2: Stage-specific transcript profiling.** (A) Pairwise scatter plots of the $\log_2$ (counts+1) for the
683 indicated samples. (B) Volcano plot (left panel) showing differential transcripts abundance between
684 two ama and pro samples as assessed by RNA-seq analysis. The dotted lines indicate fold change (FC)
685 = 2 (vertical line) and p-value = 0.01 (horizontal line). Transcripts with FC < 2 and adjusted p-value >
686 0.01 are represented by black dots. Transcripts with significant increased abundance FC ≥ 2 and
687 adjusted p-value < 0.01 in ama and pro are indicated respectively in dark cyan and dark grey. GO term
688 enrichment analysis of these transcripts for the category 'biological process' was performed, and
689 'cluster efficiency' (blue) and 'enrichment score' (orange) were plotted for the ama (middle panel) and
690 pro (right panel) datasets. The graphs show the main GO terms associated with a Benjamini and
691 Hochberg (BH) p-value < 0.05 that were identified using the BiNGO plug-in in Cytoscape. The color

692 intensity of each bar reflects the value of the BH p-value ranging from 0.05 (light blue or orange) to
693 less than 10^{-7} (dark blue or orange).
694
695 **Figure 3: Systems analysis of the stage-specific transcriptome and proteome.** (A) Volcano plot
696 showing differential protein abundance between four ama and pro samples as assessed by label-free,
697 quantitative proteomics analysis. The dotted lines indicate fold change (FC) = 2 (vertical line) and false
698 discovery rate (FDR) = 0.01 (horizontal line). Proteins with FC < 2 and FDR > 0.01 are represented by
699 light grey dots. Proteins that were reproducibly detected in only one of the two stages (considered
700 unique) are represented by the lateral histograms plotting their relative abundance according the iBAQ
701 value. These proteins together with proteins showing differential abundance of FC ≥ 2 and adjusted p-
702 value < 0.01 are indicated for ama in dark cyan and for pro in dark grey (see Table 6). GO term
703 enrichment analysis for the category 'biological process' was performed, and the resulting values for
704 'cluster efficiency' (blue) and 'enrichment score' (orange) were plotted for ama (middle panel) and pro
705 (right panel). The graphs show the main GO terms identified using the BiNGO plug-in in Cytoscape
706 and associated with a BH p-value < 0.05. The color intensity of each bar reflects the value of the BH p-
707 value ranging from 0.05 (light blue or orange) to less than 10^{-7} (dark blue or orange). (B) Double ratio
708 plot showing the log2 fold change between ama and pro in transcript (x-axis) and protein (y-axis)
709 abundances. For each dot the corresponding median absolute deviations calculated from protein and
710 transcript abundances are reported. Red dots correspond to changes in both transcript and protein
711 abundance with a p-value < 0.01. The dotted lines indicate fold changes (FC) = 2. The infinite symbol
712 (∞) represents proteins that are unique in the ama (upper signals) or pro (lower signals) datasets. Word
713 cloud enrichment performed with the *L. donovani* LdBPK orthologs is presented for each of the 4
714 quadrants, Q1 to Q4 and a detailed GO enrichment analysis is given in Table 7. The font size is
715 proportional to the number of genes per GO term and the grey scale refers to the p-value calculated for
716 each GO term. (C) KEGG map for ribosome biogenesis. Each gene associated with expression changes
717 indicated in Q1 to Q4 (see Figure 2C) and annotated with the GO term 'ribosome biogenesis' has been
718 projected on the ribosome biogenesis KEGG map. Each gene is represented by a square with the left
719 segment showing fold changes between ama and pro at transcript and the right segment showing fold

720 changes at the protein level, with the differential abundance indicated by the color and its intensity (red,
721 increase; green, decrease). Only genes quantified in both transcriptome and proteome analyses and
722 associated with an adjusted p-value < 0.01 were considered. (D) Volcano plot corresponding to the
723 differential expression of snoRNA between pro and ama stages. Cyan dots (ama) and grey dots (pro)
724 represent signals with FC ≥ 2 and adj. p-value < 0.05. Black dots represent non-significant changes. (E)
725 Localization of differentially modified rRNA sites on the *Leishmania* ribosome. The RNA
726 modifications are indicated as space filling in the *Leishmania* cryo-EM structure (PDB: 8RXH). The
727 identity of the RNA modification is defined by the label (Ψ, pseudouridine; Gm and Cm refer to guanine
728 and cytosine methylation, respectively; numbers indicate residues). Upregulated and downregulated
729 RNA modifications in amastigotes are indicated in red and blue, respectively.
730
731 **Figure 4: Analysis of stage-specific proteasomal protein turn-over.** (A) Overview of experimental
732 workflow. To assess early and late steps of differentiation (left part of the graph in black), comparative,
733 quantitative proteomics analyses were performed on tissue-isolated amastigotes (ama), amastigotes at
734 18h into the transition to promastigotes in culture (ama-18h) and fully differentiated promastigotes after
735 1 passage *in vitro* (pro). To gain insight into stage-specific and constitutive protein degradation (right
736 part of the graph in red), amastigotes and promastigotes were treated with the irreversible inhibitor
737 lactacystin (ama-lacta and pro-lacta). (B) Microscopic images of amastigotes at 18h in absence of
738 lactacystin treatment (amastigotes, left), after 48h in absence (-, middle) or presence of the inhibitor (+,
739 right). (C) Western blot analysis. Protein extracts were obtained from $2x10^6$ parasites after 3, 6, 18 and
740 48h of differentiation from amastigotes to promastigotes in presence (+) or absence (-) of lactacystin.
741 Extracts were separated by electrophoresis, transferred onto PVDF membrane and the presence of PFR2
742 was revealed using an anti-PFR2 antibody (upper panel). A Coomassie blue stain of the same gel is
743 shown as loading control (lower panel). (D) Double ratio plot comparing the log2 fold changes in
744 protein abundance between ama-18h/ama-lacta (x-axis) and ama/ama-lacta (y-axis). Dashed lines
745 indicate FC = 2 and the infinite symbol (∞) represent proteins that are unique to one or the other
746 comparison. (E) Projection of the proteins stabilized in presence of the inhibitor in ama (ama-lacta,
747 orange) and pro (pro-lacta, pink) onto the double ratio plot shown in Figure 3B. Note that ama-specific

748 proteins are rescued from degradation in pro-lacta, while pro-specific proteins are rescued from
749 degradation in ama-lacta. (F) List of the protein kinases stabilized after lactacystin treatment in pro or
750 ama (columns lacta rescued) and either not detected in the total proteome (column ama vs pro, grey
751 cell) or specifically quantified at the ama (red cell) or the pro (green cell) stage. (G) Venn diagram
752 showing the number of proteins specifically stabilized in ama or pro or stabilized in both stages after
753 lactacystin treatment.
754
755 **Figure 5: Stage-specific phospho-proteomic profiling.** (A) Volcano plots corresponding to the total
756 proteome (right panel) and phosphoproteome (left panel) analyses. Proteins and phosphosites (P-sites)
757 only identified in one stage are presented at each side of the volcano plots. Cyan dots (ama) and grey
758 dots (pro) represent signals with FC $\geq$ 2 and FDR < 1%. Light grey dots represent non-significant
759 changes. (B) Phosphostochiometry. Ratio plot comparing the log2 fold changes in total protein
760 abundance between ama and pro (x-axis) and phosphosite abundance in ama versus pro (y-axis).
761 Dashed lines indicate a FC = 2. The color intensity of each dot reflects the p-value calculated for the
762 phosphostochiometry analysis as indicated in the graph. (C) GO term enrichment analysis for the
763 category 'biological process. Only stage-specific phosphosites were considered (i.e. sites that showed
764 a significant increase in phosphostochiometry, and sites that were only detected in one or the other
765 stage, whether the protein was identified or not in the total proteome analysis). The histogram plots
766 show 'cluster efficiency' in blue and 'enrichment score' in orange for the GO term enrichment analysis
767 performed with the ama (middle panel) and pro (right panel) datasets. The main GO terms identified
768 using the BiNGO plug-in in Cytoscape and associated with a BH p-value < 0.05 are shown. The color
769 intensity of each bar reflects the value of the BH p-value ranging from 0.05 (light blue or orange) to
770 less than 10^{-7} (dark blue or orange). (D) Phosphorylation pattern of MAPK and MAPKK proteins (left
771 panel) or Ubiquitin hydrolases and transferases (right panel) identified in the phosphostochiometry
772 analysis. The positions of the phosphorylated amino acid specific to ama (red) and pro (green) are
773 indicated. Only phosphopeptides identified in the phosphostochiometry analysis (see Table 11) and
774 detected either in one stage or the other or quantified with a FC $\geq$ 2 were considered for the identification
775 of the phosphosites.

776

777 **Figure 6: Network analyses.** (A) Model of *Leishmania* gene expression regulation during stage
778 differentiation. (B-C) Network analysis. Networks, restricted to the protein kinases (blue nodes),
779 proteins implicated in ribosome biogenesis and ribosomal proteins (violet nodes) and proteins linked to
780 ubiquitination/deubiquitination (orange nodes) identified from the phosphostochiometry analysis
781 conducted in ama (B) or pro (C), were generated with the STRING plug-in of the Cytoscape software
782 package using *L. infantum* orthologs. Each node represents a phosphoprotein with the respective gene
783 identifier indicated. GO terms associated to the proteins are represented by the colored segments around
784 the nodes according to the legend shown in the graph. Only GO terms associated with a p-value < 0.05
785 were considered.

786

787 **Sup figure legends**

788 **Figure S1:** Overview of the samples used in this study. Each *L. donovani* infected hamster is identified
789 by the cage number, as are the hamster-derived amastigotes (ama) and corresponding promastigotes
790 (pro). Only samples indicated by boxes were used for the various analyses as indicated.

791

792 **Figure S2:** (A) Box plots representing the median somy score for all the chromosomes. Each box
793 corresponds to one of three biological replicates for ama and pro as indicated in the graph. Sample
794 identifiers are detailed in the legend of Figure 1A and Figure S1. (B) Frequency distribution plots
795 representing, for each biological replicate and each chromosome, a kernel density estimate of the
796 distribution of SNP frequencies in the amastigote and promastigote sample.

797

798 **Figure S3:** (A) Cluster analysis of differentially expressed genes observed from RNA sequencing
799 analysis. The heatmap is based on the variance-stabilized transformed count matrix. Rows and columns
800 have been re-ordered thanks to a hierarchical clustering (using the correlation and Euclidean distances
801 respectively and the Ward aggregation criterion). Color scale ranges from -1.5 to +1.5 as the rows of
802 the matrix have been centered.

803

804 **Figure S4:** (A) Cluster analysis of metabolites showing differential abundance in ama and pro samples.
805 (B) Quantification of amino-acids or metabolites involved in glycolysis, TCA cycle and mannogen
806 cycle. The y-axis represents the intensity for each metabolite as detected by MS. (C-D) Correlation
807 between metabolomic and proteomic analyses for TCA cycle (C) and Glycolysis/Gluconeogenesis (D).
808 Fold changes in proteins abundance (squares) and metabolite abundance (circles) with adjusted p-values
809 of respectively < 0.01 and < 0.05 were projected on the respective KEGG maps. The color intensity
810 reflects the fold change value as indicated by the legends in the graphs. (E) Representation of the
811 mannogen pathway. Metabolites are represented by a square, with red-lined squares corresponding to
812 the metabolites that accumulate at the ama stage. Proteins are represented by a circle, with fold changes
813 in protein abundance between ama and pro datasets indicated by color and intensity (red, increase;
814 green, decrease).
815
816 **Figure S5:** Label free quantitative proteomic analyses in presence or absence of lactacystin. (A) to (E)
817 Volcano plots representing changes in protein abundance for the different comparisons (left panels) and
818 GO term enrichment analyses for the indicated sample (right panels). Proteins identified by at least two
819 peptides in at least three out of four biological replicates were considered. For volcano plots, colored
820 dots indicate values with FDR < 0.01 and FC ≥ 2 (see Table 8). The light grey dots indicate non-
821 significant expression changes. The colored bars indicate unique protein identifications in one (green)
822 or the other (orange) condition with relative abundance indicated by the iBAQ value (left panels).
823 Proteins quantified in only one condition or showing a significant increase in abundance (FC ≥ 2 and
824 adjusted p-value < 0.01) were used to perform the GO analysis for the category 'biological process'.
825 The histogram plots show 'cluster efficiency' in blue and 'enrichment score' in orange (right panels).
826 (A) ama vs ama-18h; (B) ama-18h vs pro; (C) ama vs ama lacta; (D) ama-18h vs ama lacta; (E) pro vs
827 pro lacta.
828
829 **Figure S6:** (A) Functional network enrichment analysis for proteins showing increased abundance in
830 ama-18h compared to ama. The network was generated with the *L. infantum* orthologs using the
831 STRING plug-in of the Cytoscape software package. The GO terms associated with each protein are

832 represented by the colored segments according to the legend. Only GO terms associated with a p-value
833 < 0.05 were considered. (B) KEGG map for ribosome biogenesis showing changes in abundance protein
834 between ama and ama-18h. Only proteins with an adjusted p-value < 0.01 were considered. Differential
835 abundance is indicated by the color and its intensity (red, increase; green, decrease).
836
837 **Figure S7:** (A) Viability assessment of the indicated amastigote (left panel) and promastigote (right
838 panel) samples after lactacystin treatment by FACS analysis using propidium iodide or YoPro staining.
839 (B) Micrographs showing hamster-derived amastigotes during *in vitro* differentiation to promastigotes.
840 Parasites were collected at the time points indicated, fixed in 4% PFA, and seeded on poly-L-lysine-
841 treated coverslips. Parasites were observed with a 63x oil immersion objective and images were
842 processed with AxioVision Rel.4.8 software. Differential interference contrast (DIC) microscopy was
843 performed with Axioplan 2 imaging microscope using a 63x oil immersion objective, Axiovision
844 software and AxioCam MRm camera (Carl Zeiss). The scale bars correspond to 1 µm. (C) Western blot
845 analysis of protein extracts obtained at the indicated time points after *in vitro* differentiation from
846 hamster-derived amastigotes to promastigotes. 10 µg of protein were separated on NuPAGE 4-12%,
847 transferred onto PVDF membrane subsequently incubated with antibodies against paraflagellar rod
848 proteins 1 and 2 and alpha-tubulin, and revealed with HRP-conjugated secondary antibodies.
849
850 **Figure S8:** Functional network enrichment analysis for the proteins stabilized in presence of lactacystin
851 in promastigote (pro) and amastigote (ama) datasets. The network was generated with the *L. infantum*
852 orthologs using the STRING plug-in of the Cytoscape software package. The GO terms associated with
853 each protein are represented by the coloured segments according to the legend. Only GO terms
854 associated with a p-value < 0.05 were considered.
855
856 **Figure S9:** List of protein kinases stabilized in presence of lactacystin. Their corresponding orthologs
857 in *L. donovani* strain LdBPK and *L. mexicana* are indicated, as well as the knock-out phenotype as
858 published by Baker et al (2021).
859

860 **Figure S10:** Upset plot representing the number of phosphopeptides (y-axis, blue histograms, numbers
861 are indicated) and the samples in which they were quantified (x-axis). Pie chart of the phosphopeptide
862 analysis showing the distribution of the phosphorylation sites according to the condition in which they
863 were quantified as indicated in the legend of the graph.
864
865 **Figure S11:** Functional Network analysis. Networks for proteins that show unique or increased
866 phosphorylation in ama (upper panel) and in pro (lower panel) datasets were generated with the
867 STRING plug-in of the Cytoscape software package using *L. infantum* orthologs. The nodes represent
868 phosphoproteins associated with one or more GO terms (listed in the graph), with the respective gene
869 identifier indicated. The GO terms associated to the proteins are represented by the colored segments
870 around the nodes according to the legend shown in the graph. Only GO terms associated with a p-value
871 < 0.05 were considered.
872
873
874
875

Acknowledgments

We thank the CEA-CNRGH for its contribution to the sequencing costs and all the CEA-CNRGH staff who performed sample preparation and sequencing for their excellent technical assistance.

We acknowledge the help of the HPC Core Facility of the Institut Pasteur for this work.

We thank Karim Sébastien from the animal facility of the Institut Pasteur for his commitment in the care of our animals.

This work was supported by the Agence Nationale pour la Recherche Labex 'Integrative Biology of Emerging Infectious Diseases' contract ANR-10-LABX-62-IBEID and Labex 'French Alliance for Parasitology and Health Care' contract ANR-11-LABX-0024 (GFS, PP), the France Génomique National infrastructure, funded as part of the « Investissements d'Avenir » program managed by the Agence Nationale pour la Recherche contract ANR-10-INBS-09 (HV, RL, CP), and the ERC SYNERGY project DecoLeishRN, Grant agreement ID: 101071613.

889 **REFERENCES**

890

891

892 1. Hollin T, Le Roch KG. From Genes to Transcripts, a Tightly Regulated Journey in Plasmodium.
893 Frontiers in cellular and infection microbiology. 2020;10:618454. doi: 10.3389/fcimb.2020.618454.
894 PubMed PMID: 33425787; PubMed Central PMCID: PMC7793691.
895 2. Modrzynska K, Pfander C, Chappell L, Yu L, Suarez C, Dundas K, Gomes AR, Goulding D,
896 Rayner JC, Choudhary J, Billker O. A Knockout Screen of ApiAP2 Genes Reveals Networks of
897 Interacting Transcriptional Regulators Controlling the Plasmodium Life Cycle. Cell host & microbe.
898 2017;21(1):11-22. doi: 10.1016/j.chom.2016.12.003. PubMed PMID: 28081440; PubMed Central
899 PMCID: PMC5241200.
900 3. Waldman BS, Schwarz D, Wadsworth MH, 2nd, Saeij JP, Shalek AK, Lourido S. Identification
901 of a Master Regulator of Differentiation in Toxoplasma. Cell. 2020;180(2):359-72 e16. doi:
902 10.1016/j.cell.2019.12.013. PubMed PMID: 31955846; PubMed Central PMCID: PMC6978799.
903 4. Alvar J, Velez ID, Bern C, Herrero M, Desjeux P, Cano J, Jannin J, den Boer M, Team
904 WHOLC. Leishmaniasis worldwide and global estimates of its incidence. PloS one. 2012;7(5):e35671.
905 doi: 10.1371/journal.pone.0035671. PubMed PMID: 22693548; PubMed Central PMCID:
906 PMC3365071.
907 5. WHO. Leishmaniasis 2023. Available from: https://www.who.int/news-room/fact-
908 sheets/detail/leishmaniasis.
909 6. Maia C, Conceicao C, Pereira A, Rocha R, Ortuno M, Munoz C, Jumakanova Z, Perez-Cutillas
910 P, Ozbel Y, Toz S, Baneth G, Monge-Maillo B, Gasimov E, Van der Stede Y, Torres G, Gossner CM,
911 Berriatua E. The estimated distribution of autochthonous leishmaniasis by Leishmania infantum in
912 Europe in 2005-2020. PLoS neglected tropical diseases. 2023;17(7):e0011497. doi:
913 10.1371/journal.pntd.0011497. PubMed PMID: 37467280; PubMed Central PMCID: PMC10389729.
914 7. Barbiero A, Spinicci M, Aiello A, Maruotto M, Antonello RM, Formica G, Piccica M, Isola P,
915 Parisio EM, Nardone M, Valentini S, Mangano V, Brunelli T, Bianchi L, Bartalesi F, Costa C, Sambo
916 M, Tumbarello M, Sani S, Fabiani S, Rossetti B, Nencioni C, Lanari A, Aquilini D, Montorzi G,
917 Venturini E, Galli L, Rinninella G, Falcone M, Ceriegi F, Amadori F, Vincenti A, Blanc P, Vellere I,
918 Tacconi D, Luchi S, Moneta S, Massi D, Brogi M, Voller F, Gemmi F, Rossolini GM, Cusi MG, Bruschi
919 F, Bartoloni A, Zammarchi L. The Uprise of Human Leishmaniasis in Tuscany, Central Italy: Clinical
920 and Epidemiological Data from a Multicenter Study. Microorganisms. 2024;12(10). doi:
921 10.3390/microorganisms12101963. PubMed PMID: 39458272; PubMed Central PMCID:
922 PMC11509187.
923 8. Handman E. Cell biology of Leishmania. Advances in parasitology. 1999;44:1-39. doi:
924 10.1016/s0065-308x(08)60229-8. PubMed PMID: 10563394.
925 9. Clayton CE. Life without transcriptional control? From fly to man and back again. The EMBO
926 journal. 2002;21(8):1881-8. doi: 10.1093/emboj/21.8.1881. PubMed PMID: 11953307; PubMed
927 Central PMCID: PMC125970.
928 10. Liang XH, Haritan A, Uliel S, Michaeli S. trans and cis splicing in trypanosomatids:
929 mechanism, factors, and regulation. Eukaryotic cell. 2003;2(5):830-40. doi: 10.1128/EC.2.5.830-
930 840.2003. PubMed PMID: 14555465; PubMed Central PMCID: PMC219355.
931 11. McConville MJ, Ralton JE. Developmentally regulated changes in the cell surface architecture
932 of Leishmania parasites. Behring Institute Mitteilungen. 1997(99):34-43. PubMed PMID: 9303200.
933 12. McConville MJ, de Souza D, Saunders E, Likic VA, Naderer T. Living in a phagolysosome;
934 metabolism of Leishmania amastigotes. Trends in parasitology. 2007;23(8):368-75. doi:
935 10.1016/j.pt.2007.06.009. PubMed PMID: 17606406.
936 13. Rosenzweig D, Smith D, Opperdoes F, Stern S, Olafson RW, Zilberstein D. Retooling
937 Leishmania metabolism: from sand fly gut to human macrophage. FASEB journal : official publication
938 of the Federation of American Societies for Experimental Biology. 2008;22(2):590-602. doi:
939 10.1096/fj.07-9254com. PubMed PMID: 17884972.

14. McConville MJ, Naderer T. Metabolic pathways required for the intracellular survival of Leishmania. Annual review of microbiology. 2011;65:543-61. doi: 10.1146/annurev-micro-090110-102913. PubMed PMID: 21721937.
15. Sunter J, Gull K. Shape, form, function and Leishmania pathogenicity: from textbook descriptions to biological understanding. Open biology. 2017;7(9). doi: 10.1098/rsob.170165. PubMed PMID: 28903998; PubMed Central PMCID: PMC5627057.
16. Dandugudumula R, Fischer-Weinberger R, Zilberstein D. Morphogenesis Dynamics in Leishmania Differentiation. Pathogens. 2022;11(9). doi: 10.3390/pathogens11090952. PubMed PMID: 36145385; PubMed Central PMCID: PMC9505065.
17. Trenaman A, Glover L, Hutchinson S, Horn D. A post-transcriptional respiratome regulon in trypanosomes. Nucleic acids research. 2019;47(13):7063-77. doi: 10.1093/nar/gkz455. PubMed PMID: 31127277; PubMed Central PMCID: PMC6648352.
18. Boucher N, Wu Y, Dumas C, Dube M, Sereno D, Breton M, Papadopoulou B. A common mechanism of stage-regulated gene expression in Leishmania mediated by a conserved 3'-untranslated region element. The Journal of biological chemistry. 2002;277(22):19511-20. doi: 10.1074/jbc.M200500200. PubMed PMID: 11912202.
19. McNicoll F, Muller M, Cloutier S, Boilard N, Rochette A, Dube M, Papadopoulou B. Distinct 3'-untranslated region elements regulate stage-specific mRNA accumulation and translation in Leishmania. The Journal of biological chemistry. 2005;280(42):35238-46. doi: 10.1074/jbc.M507511200. PubMed PMID: 16115874.
20. Bringaud F, Muller M, Cerqueira GC, Smith M, Rochette A, El-Sayed NM, Papadopoulou B, Ghedin E. Members of a large retroposon family are determinants of post-transcriptional gene expression in Leishmania. PLoS pathogens. 2007;3(9):1291-307. doi: 10.1371/journal.ppat.0030136. PubMed PMID: 17907803; PubMed Central PMCID: PMC2323293.
21. Azizi H, Dumas C, Papadopoulou B. The Pumilio-domain protein PUF6 contributes to SIDER2 retroposon-mediated mRNA decay in Leishmania. Rna. 2017;23(12):1874-85. doi: 10.1261/rna.062950.117. PubMed PMID: 28877997; PubMed Central PMCID: PMC5689007.
22. Clayton C, Estevez A. The exosomes of trypanosomes and other protists. Advances in experimental medicine and biology. 2011;702:39-49. doi: 10.1007/978-1-4419-7841-7_4. PubMed PMID: 21713676.
23. Schwede A, Manful T, Jha BA, Helbig C, Bercovich N, Stewart M, Clayton C. The role of deadenylation in the degradation of unstable mRNAs in trypanosomes. Nucleic acids research. 2009;37(16):5511-28. doi: 10.1093/nar/gkp571. PubMed PMID: 19596809; PubMed Central PMCID: PMC2760810.
24. Kramer S. The ApaH-like phosphatase TbALPH1 is the major mRNA decapping enzyme of trypanosomes. PLoS pathogens. 2017;13(6):e1006456. doi: 10.1371/journal.ppat.1006456. PubMed PMID: 28628654; PubMed Central PMCID: PMC5491325.
25. Yoffe Y, Zuberek J, Lewdorowicz M, Zeira Z, Keasar C, Orr-Dahan I, Jankowska-Anyszka M, Stepinski J, Darzynkiewicz E, Shapira M. Cap-binding activity of an eIF4E homolog from Leishmania. Rna. 2004;10(11):1764-75. doi: 10.1261/rna.7520404. PubMed PMID: 15388875; PubMed Central PMCID: PMC1370664.
26. Yoffe Y, Zuberek J, Lerer A, Lewdorowicz M, Stepinski J, Altmann M, Darzynkiewicz E, Shapira M. Binding specificities and potential roles of isoforms of eukaryotic initiation factor 4E in Leishmania. Eukaryotic cell. 2006;5(12):1969-79. doi: 10.1128/EC.00230-06. PubMed PMID: 17041189; PubMed Central PMCID: PMC1694823.
27. David M, Gabdank I, Ben-David M, Zilka A, Orr I, Barash D, Shapira M. Preferential translation of Hsp83 in Leishmania requires a thermosensitive polypyrimidine-rich element in the 3' UTR and involves scanning of the 5' UTR. Rna. 2010;16(2):364-74. doi: 10.1261/rna.1874710. PubMed PMID: 20040590; PubMed Central PMCID: PMC2811665.
28. Freire ER, Sturm NR, Campbell DA, de Melo Neto OP. The Role of Cytoplasmic mRNA Cap-Binding Protein Complexes in Trypanosoma brucei and Other Trypanosomatids. Pathogens. 2017;6(4). doi: 10.3390/pathogens6040055. PubMed PMID: 29077018; PubMed Central PMCID: PMC5750579.
29. Shrivastava R, Tupperwar N, Schwartz B, Baron N, Shapira M. LeishIF4E-5 Is a Promastigote-Specific Cap-Binding Protein in Leishmania. International journal of molecular sciences. 2021;22(8). doi: 10.3390/ijms22083979. PubMed PMID: 33921489; PubMed Central PMCID: PMC8069130.

30. Assis LA, Santos Filho MVC, da Cruz Silva JR, Bezerra MJR, de Aquino I, Merlo KC, Holetz FB, Probst CM, Rezende AM, Papadopoulou B, da Costa Lima TDC, de Melo Neto OP. Identification of novel proteins and mRNAs differentially bound to the Leishmania Poly(A) Binding Proteins reveals a direct association between PABP1, the RNA-binding protein RBP23 and mRNAs encoding ribosomal proteins. PLoS neglected tropical diseases. 2021;15(10):e0009899. doi: 10.1371/journal.pntd.0009899. PubMed PMID: 34705820; PubMed Central PMCID: PMC8575317 competing interests.
31. Piel L, Rajan KS, Bussotti G, Varet H, Legendre R, Proux C, Douche T, Giai-Gianetto Q, Chaze T, Cokelaer T, Vojtkova B, Gordon-Bar N, Doniger T, Cohen-Chalamish S, Rengaraj P, Besse C, Boland A, Sadlova J, Deleuze JF, Matondo M, Unger R, Volf P, Michaeli S, Pescher P, Spath GF. Experimental evolution links post-transcriptional regulation to Leishmania fitness gain. PLoS pathogens. 2022;18(3):e1010375. doi: 10.1371/journal.ppat.1010375. PubMed PMID: 35294501; PubMed Central PMCID: PMC8959184.
32. Rodriguez-Almonacid CC, Kellogg MK, Karamyshev AL, Karamysheva ZN. Ribosome Specialization in Protozoa Parasites. International journal of molecular sciences. 2023;24(8). doi: 10.3390/ijms24087484. PubMed PMID: 37108644; PubMed Central PMCID: PMC10138883.
33. Gutierrez Guarnizo SA, Tikhonova EB, Karamyshev AL, Muskus CE, Karamysheva ZN. Translational reprogramming as a driver of antimony-drug resistance in Leishmania. Nature communications. 2023;14(1):2605. doi: 10.1038/s41467-023-38221-1. PubMed PMID: 37147291; PubMed Central PMCID: PMC10163012.
34. Rajan KS, Aryal S, Hiregange DG, Bashan A, Madmoni H, Olami M, Doniger T, Cohen-Chalamish S, Pescher P, Taoka M, Nobe Y, Fedorenko A, Bose T, Zimermann E, Prina E, Aharon-Hefetz N, Pilpel Y, Isobe T, Unger R, Spath GF, Yonath A, Michaeli S. Structural and mechanistic insights into the function of Leishmania ribosome lacking a single pseudouridine modification. Cell reports. 2024;43(5):114203. doi: 10.1016/j.celrep.2024.114203. PubMed PMID: 38722744.
35. Besteiro S, Williams RA, Morrison LS, Coombs GH, Mottram JC. Endosome sorting and autophagy are essential for differentiation and virulence of Leishmania major. The Journal of biological chemistry. 2006;281(16):11384-96. doi: 10.1074/jbc.M512307200. PubMed PMID: 16497676.
36. Williams RA, Tetley L, Mottram JC, Coombs GH. Cysteine peptidases CPA and CPB are vital for autophagy and differentiation in Leishmania mexicana. Molecular microbiology. 2006;61(3):655-74. doi: 10.1111/j.1365-2958.2006.05274.x. PubMed PMID: 16803590.
37. Besteiro S, Williams RA, Coombs GH, Mottram JC. Protein turnover and differentiation in Leishmania. International journal for parasitology. 2007;37(10):1063-75. doi: 10.1016/j.ijpara.2007.03.008. PubMed PMID: 17493624; PubMed Central PMCID: PMC2244715.
38. Williams RA, Smith TK, Cull B, Mottram JC, Coombs GH. ATG5 is essential for ATG8-dependent autophagy and mitochondrial homeostasis in Leishmania major. PLoS pathogens. 2012;8(5):e1002695. doi: 10.1371/journal.ppat.1002695. PubMed PMID: 22615560; PubMed Central PMCID: PMC3355087.
39. Williams RA, Mottram JC, Coombs GH. Distinct roles in autophagy and importance in infectivity of the two ATG4 cysteine peptidases of Leishmania major. The Journal of biological chemistry. 2013;288(5):3678-90. doi: 10.1074/jbc.M112.415372. PubMed PMID: 23166325; PubMed Central PMCID: PMC3561585.
40. Sakamoto H, Nakada-Tsukui K, Besteiro S. The Autophagy Machinery in Human-Parasitic Protists; Diverse Functions for Universally Conserved Proteins. Cells. 2021;10(5). doi: 10.3390/cells10051258. PubMed PMID: 34069694; PubMed Central PMCID: PMC8161075.
41. Casgrain PA, Martel C, McMaster WR, Mottram JC, Olivier M, Descoteaux A. Cysteine Peptidase B Regulates Leishmania mexicana Virulence through the Modulation of GP63 Expression. PLoS pathogens. 2016;12(5):e1005658. doi: 10.1371/journal.ppat.1005658. PubMed PMID: 27191844; PubMed Central PMCID: PMC4871588.
42. Pescher P, Blisnick T, Bastin P, Spath GF. Quantitative proteome profiling informs on phenotypic traits that adapt Leishmania donovani for axenic and intracellular proliferation. Cellular microbiology. 2011;13(7):978-91. doi: 10.1111/j.1462-5822.2011.01593.x. PubMed PMID: 21501362.
43. Li H, Handsaker B, Wysoker A, Fennell T, Ruan J, Homer N, Marth G, Abecasis G, Durbin R, Genome Project Data Processing S. The Sequence Alignment/Map format and SAMtools. Bioinformatics. 2009;25(16):2078-9. doi: 10.1093/bioinformatics/btp352. PubMed PMID: 19505943; PubMed Central PMCID: PMC2723002.

44. DePristo MA, Banks E, Poplin R, Garimella KV, Maguire JR, Hartl C, Philippakis AA, del Angel G, Rivas MA, Hanna M, McKenna A, Fennell TJ, Kernytsky AM, Sivachenko AY, Cibulskis K, Gabriel SB, Altshuler D, Daly MJ. A framework for variation discovery and genotyping using next-generation DNA sequencing data. Nature genetics. 2011;43(5):491-8. doi: 10.1038/ng.806. PubMed PMID: 21478889; PubMed Central PMCID: PMC3083463.
45. Quinlan AR, Hall IM. BEDTools: a flexible suite of utilities for comparing genomic features. Bioinformatics. 2010;26(6):841-2. doi: 10.1093/bioinformatics/btq033. PubMed PMID: 20110278; PubMed Central PMCID: PMC2832824.
46. Prieto Barja P, Pescher P, Bussotti G, Dumetz F, Imamura H, Kedra D, Domagalska M, Chaumeau V, Himmelbauer H, Pages M, Sterkers Y, Dujardin JC, Notredame C, Spath GF. Haplotype selection as an adaptive mechanism in the protozoan pathogen Leishmania donovani. Nature ecology & evolution. 2017;1(12):1961-9. doi: 10.1038/s41559-017-0361-x. PubMed PMID: 29109466.
47. Liao Y, Smyth GK, Shi W. featureCounts: an efficient general purpose program for assigning sequence reads to genomic features. Bioinformatics. 2014;30(7):923-30. doi: 10.1093/bioinformatics/btt656. PubMed PMID: 24227677.
48. Spath GF, Bussotti G. GIP: an open-source computational pipeline for mapping genomic instability from protists to cancer cells. Nucleic acids research. 2022;50(6):e36. doi: 10.1093/nar/gkab1237. PubMed PMID: 34928370; PubMed Central PMCID: PMC8989552.
49. Cokelaer T. Sequana': a Set of Snakemake NGS pipelines. Journal of Open Source Software. 2017;2(16). doi: 10.21105/joss.00352.
50. Martin M. Cutadapt removes adapter sequences from high-throughput sequencing reads. EMBnetjournal. 2011;17(1). doi: 10.14806/ej.17.1.200.
51. Dobin A, Davis CA, Schlesinger F, Drenkow J, Zaleski C, Jha S, Batut P, Chaisson M, Gingeras TR. STAR: ultrafast universal RNA-seq aligner. Bioinformatics. 2013;29(1):15-21. doi: 10.1093/bioinformatics/bts635. PubMed PMID: 23104886; PubMed Central PMCID: PMC3530905.
52. Team RC. R: A Language and Environment for Statistical Computing. R Foundation for Statistical Computing2016.
53. Love MI, Huber W, Anders S. Moderated estimation of fold change and dispersion for RNA-seq data with DESeq2. Genome biology. 2014;15(12):550. doi: 10.1186/s13059-014-0550-8. PubMed PMID: 25516281; PubMed Central PMCID: PMC4302049.
54. Benjamini YHY. Controlling the False Discovery Rate: A Practical and Powerful Approach to Multiple Testing. Journal of the Royal Statistical Society: Series B (Methodological). 1995;57(1):289-300. doi: 10.1111/j.2517-6161.1995.tb02031.x.
55. Erde J, Loo RR, Loo JA. Enhanced FASP (eFASP) to increase proteome coverage and sample recovery for quantitative proteomic experiments. Journal of proteome research. 2014;13(4):1885-95. doi: 10.1021/pr4010019. PubMed PMID: 24552128; PubMed Central PMCID: PMC3993969.
56. Matheron L, van den Toorn H, Heck AJ, Mohammed S. Characterization of biases in phosphopeptide enrichment by Ti(4+)-immobilized metal affinity chromatography and TiO2 using a massive synthetic library and human cell digests. Analytical chemistry. 2014;86(16):8312-20. doi: 10.1021/ac501803z. PubMed PMID: 25068997.
57. Creek DJ, Jankevics A, Burgess KE, Breitling R, Barrett MP. IDEOM: an Excel interface for analysis of LC-MS-based metabolomics data. Bioinformatics. 2012;28(7):1048-9. doi: 10.1093/bioinformatics/bts069. PubMed PMID: 22308147.
58. Scheltema RA, Jankevics A, Jansen RC, Swertz MA, Breitling R. PeakML/mzMatch: a file format, Java library, R library, and tool-chain for mass spectrometry data analysis. Analytical chemistry. 2011;83(7):2786-93. doi: 10.1021/ac2000994. PubMed PMID: 21401061.
59. Pettersen EF, Goddard TD, Huang CC, Meng EC, Couch GS, Croll TI, Morris JH, Ferrin TE. UCSF ChimeraX: Structure visualization for researchers, educators, and developers. Protein science : a publication of the Protein Society. 2021;30(1):70-82. doi: 10.1002/pro.3943. PubMed PMID: 32881101; PubMed Central PMCID: PMC7737788.
60. Bussotti G, Piel L, Pescher P, Domagalska MA, Rajan KS, Cohen-Chalamish S, Doniger T, Hiregange DG, Myler PJ, Unger R, Michaeli S, Spath GF. Genome instability drives epistatic adaptation in the human pathogen Leishmania. Proceedings of the National Academy of Sciences of the United States of America. 2021;118(51). doi: 10.1073/pnas.2113744118. PubMed PMID: 34903666; PubMed Central PMCID: PMC8713814.

1105 61. Perez-Riverol Y, Csordas A, Bai J, Bernal-Llinares M, Hewapathirana S, Kundu DJ, Inuganti
1106 A, Griss J, Mayer G, Eisenacher M, Perez E, Uszkoreit J, Pfeuffer J, Sachsenberg T, Yilmaz S, Tiwary
1107 S, Cox J, Audain E, Walzer M, Jarnuczak AF, Ternent T, Brazma A, Vizcaino JA. The PRIDE database
1108 and related tools and resources in 2019: improving support for quantification data. Nucleic acids
1109 research. 2019;47(D1):D442-D50. doi: 10.1093/nar/gky1106. PubMed PMID: 30395289; PubMed
1110 Central PMCID: PMC6323896.
1111 62. Edgar R, Domrachev M, Lash AE. Gene Expression Omnibus: NCBI gene expression and
1112 hybridization array data repository. Nucleic acids research. 2002;30(1):207-10. doi:
1113 10.1093/nar/30.1.207. PubMed PMID: 11752295; PubMed Central PMCID: PMC99122.
1114 63. Bussotti G, Li B, Pescher P, Vojtkova B, Louradour I, Pruzinova K, Sadlova J, Volf P, Spath
1115 GF. Leishmania allelic selection during experimental sand fly infection correlates with mutational
1116 signatures of oxidative DNA damage. Proceedings of the National Academy of Sciences of the United
1117 States of America. 2023;120(10):e2220828120. doi: 10.1073/pnas.2220828120. PubMed PMID:
1118 36848551; PubMed Central PMCID: PMC10013807.
1119 64. Marques CA, Dickens NJ, Paape D, Campbell SJ, McCulloch R. Genome-wide mapping
1120 reveals single-origin chromosome replication in Leishmania, a eukaryotic microbe. Genome biology.
1121 2015;16:230. doi: 10.1186/s13059-015-0788-9. PubMed PMID: 26481451; PubMed Central PMCID:
1122 PMC4612428.
1123 65. Bussotti G, Gouzelou E, Cortes Boite M, Kherachi I, Harrat Z, Eddaikra N, Mottram JC,
1124 Antoniou M, Christodoulou V, Bali A, Guerfali FZ, Laouini D, Mukhtar M, Dumetz F, Dujardin JC,
1125 Smirlis D, Lechat P, Pescher P, El Hamouchi A, Lemrani M, Chicharro C, Llanes-Acevedo IP, Botana
1126 L, Cruz I, Moreno J, Jeddi F, Aoun K, Bouratbine A, Cupolillo E, Spath GF. Leishmania Genome
1127 Dynamics during Environmental Adaptation Reveal Strain-Specific Differences in Gene Copy Number
1128 Variation, Karyotype Instability, and Telomeric Amplification. mBio. 2018;9(6). doi:
1129 10.1128/mBio.01399-18. PubMed PMID: 30401775; PubMed Central PMCID: PMC6222132.
1130 66. Kloehn J, Saunders EC, O'Callaghan S, Dagley MJ, McConville MJ. Characterization of
1131 metabolically quiescent Leishmania parasites in murine lesions using heavy water labeling. PLoS
1132 pathogens. 2015;11(2):e1004683. doi: 10.1371/journal.ppat.1004683. PubMed PMID: 25714830;
1133 PubMed Central PMCID: PMC4340956.
1134 67. Bussotti G, Benkahla A, Jeddi F, Souiai O, Aoun K, Spath GF, Bouratbine A. Nuclear and
1135 mitochondrial genome sequencing of North-African Leishmania infantum isolates from cured and
1136 relapsed visceral leishmaniasis patients reveals variations correlating with geography and phenotype.
1137 Microbial genomics. 2020;6(10). doi: 10.1099/mgen.0.000444. PubMed PMID: 32975503; PubMed
1138 Central PMCID: PMC7660250.
1139 68. Dumetz F, Imamura H, Sanders M, Seblova V, Myskova J, Pescher P, Vanaerschot M, Meehan
1140 CJ, Cuypers B, De Muylder G, Spath GF, Bussotti G, Vermeesch JR, Berriman M, Cotton JA, Volf P,
1141 Dujardin JC, Domagalska MA. Modulation of Aneuploidy in Leishmania donovani during Adaptation
1142 to Different In Vitro and In Vivo Environments and Its Impact on Gene Expression. mBio. 2017;8(3).
1143 doi: 10.1128/mBio.00599-17. PubMed PMID: 28536289; PubMed Central PMCID: PMC5442457.
1144 69. Wu Y, El Fakhry Y, Sereno D, Tamar S, Papadopoulou B. A new developmentally regulated
1145 gene family in Leishmania amastigotes encoding a homolog of amastin surface proteins. Molecular and
1146 biochemical parasitology. 2000;110(2):345-57. doi: 10.1016/s0166-6851(00)00290-5. PubMed PMID:
1147 11071288.
1148 70. Haile S, Dupe A, Papadopoulou B. Deadenylation-independent stage-specific mRNA
1149 degradation in Leishmania. Nucleic acids research. 2008;36(5):1634-44. doi: 10.1093/nar/gkn019.
1150 PubMed PMID: 18250085; PubMed Central PMCID: PMC2275140.
1151 71. Fiebig M, Kelly S, Gluenz E. Comparative Life Cycle Transcriptomics Revises Leishmania
1152 mexicana Genome Annotation and Links a Chromosome Duplication with Parasitism of Vertebrates.
1153 PLoS pathogens. 2015;11(10):e1005186. doi: 10.1371/journal.ppat.1005186. PubMed PMID:
1154 26452044; PubMed Central PMCID: PMC4599935.
1155 72. Saunders EC, Sernee MF, Ralton JE, McConville MJ. Metabolic stringent response in
1156 intracellular stages of Leishmania. Current opinion in microbiology. 2021;63:126-32. doi:
1157 10.1016/j.mib.2021.07.007. PubMed PMID: 34340099.
1158 73. Sernee MF, Ralton JE, Nero TL, Sobala LF, Kloehn J, Vieira-Lara MA, Cobbold SA, Stanton
1159 L, Pires DEV, Hanssen E, Males A, Ward T, Bastidas LM, van der Peet PL, Parker MW, Ascher DB,

1160 Williams SJ, Davies GJ, McConville MJ. A Family of Dual-Activity Glycosyltransferase-
1161 Phosphorylases Mediates Mannogen Turnover and Virulence in Leishmania Parasites. Cell host &
1162 microbe. 2019;26(3):385-99 e9. doi: 10.1016/j.chom.2019.08.009. PubMed PMID: 31513773.
1163 74. Omura S, Crump A. Lactacystin: first-in-class proteasome inhibitor still excelling and an
1164 exemplar for future antibiotic research. The Journal of antibiotics. 2019;72(4):189-201. doi:
1165 10.1038/s41429-019-0141-8. PubMed PMID: 30755736; PubMed Central PMCID: PMC6760633.
1166 75. Kumar P, Sundar S, Singh N. Degradation of pteridine reductase 1 (PTR1) enzyme during
1167 growth phase in the protozoan parasite Leishmania donovani. Experimental parasitology.
1168 2007;116(2):182-9. doi: 10.1016/j.exppara.2006.12.008. PubMed PMID: 17275814.
1169 76. Perez-Pertejo Y, Alvarez-Velilla R, Estrada CG, Balana-Fouce R, Reguera RM. Leishmania
1170 donovani: proteasome-mediated down-regulation of methionine adenosyltransferase. Parasitology.
1171 2011;138(9):1082-92. doi: 10.1017/S0031182011000862. PubMed PMID: 21813028.
1172 77. Vince JE, Tull D, Landfear S, McConville MJ. Lysosomal degradation of Leishmania hexose
1173 and inositol transporters is regulated in a stage-, nutrient- and ubiquitin-dependent manner. International
1174 journal for parasitology. 2011;41(7):791-800. doi: 10.1016/j.ijpara.2011.02.003. PubMed PMID:
1175 21447343; PubMed Central PMCID: PMC3592973.
1176 78. Khare S, Nagle AS, Biggart A, Lai YH, Liang F, Davis LC, Barnes SW, Mathison CJ, Myburgh
1177 E, Gao MY, Gillespie JR, Liu X, Tan JL, Stinson M, Rivera IC, Ballard J, Yeh V, Groessl T, Federe G,
1178 Koh HX, Venable JD, Bursulaya B, Shapiro M, Mishra PK, Spraggon G, Brock A, Mottram JC,
1179 Buckner FS, Rao SP, Wen BG, Walker JR, Tuntland T, Molteni V, Glynne RJ, Supek F. Proteasome
1180 inhibition for treatment of leishmaniasis, Chagas disease and sleeping sickness. Nature.
1181 2016;537(7619):229-33. doi: 10.1038/nature19339. PubMed PMID: 27501246; PubMed Central
1182 PMCID: PMC5161665.
1183 79. Wyllie S, Brand S, Thomas M, De Rycker M, Chung CW, Pena I, Bingham RP, Bueren-
1184 Calabuig JA, Cantizani J, Cebrian D, Craggs PD, Ferguson L, Goswami P, Hobrath J, Howe J, Jeacock
1185 L, Ko EJ, Korczynska J, MacLean L, Manthri S, Martinez MS, Mata-Cantero L, Moniz S, Nuhs A,
1186 Osuna-Cabello M, Pinto E, Riley J, Robinson S, Rowland P, Simeons FRC, Shishikura Y, Spinks D,
1187 Stojanovski L, Thomas J, Thompson S, Viayna Gaza E, Wall RJ, Zuccotto F, Horn D, Ferguson MAJ,
1188 Fairlamb AH, Fiandor JM, Martin J, Gray DW, Miles TJ, Gilbert IH, Read KD, Marco M, Wyatt PG.
1189 Preclinical candidate for the treatment of visceral leishmaniasis that acts through proteasome inhibition.
1190 Proceedings of the National Academy of Sciences of the United States of America. 2019;116(19):9318-
1191 23. doi: 10.1073/pnas.1820175116. PubMed PMID: 30962368; PubMed Central PMCID:
1192 PMC6511062.
1193 80. Burge RJ, Damianou A, Wilkinson AJ, Rodenko B, Mottram JC. Leishmania differentiation
1194 requires ubiquitin conjugation mediated by a UBC2-UEV1 E2 complex. PLoS pathogens.
1195 2020;16(10):e1008784. doi: 10.1371/journal.ppat.1008784. PubMed PMID: 33108402; PubMed
1196 Central PMCID: PMC7647121.
1197 81. Damianou A, Burge RJ, Catta-Preta CMC, Geoghegan V, Nievas YR, Newling K, Brown E,
1198 Burchmore R, Rodenko B, Mottram JC. Essential roles for deubiquitination in Leishmania life cycle
1199 progression. PLoS pathogens. 2020;16(6):e1008455. doi: 10.1371/journal.ppat.1008455. PubMed
1200 PMID: 32544189; PubMed Central PMCID: PMC7319358.
1201 82. Parsons M, Worthey EA, Ward PN, Mottram JC. Comparative analysis of the kinomes of three
1202 pathogenic trypanosomatids: Leishmania major, Trypanosoma brucei and Trypanosoma cruzi. BMC
1203 genomics. 2005;6:127. doi: 10.1186/1471-2164-6-127. PubMed PMID: 16164760; PubMed Central
1204 PMCID: PMC1266030.
1205 83. Morales MA, Renaud O, Faigle W, Shorte SL, Spath GF. Over-expression of Leishmania major
1206 MAP kinases reveals stage-specific induction of phosphotransferase activity. International journal for
1207 parasitology. 2007;37(11):1187-99. doi: 10.1016/j.ijpara.2007.03.006. PubMed PMID: 17481635.
1208 84. Rotureau B, Morales MA, Bastin P, Spath GF. The flagellum-mitogen-activated protein kinase
1209 connection in Trypanosomatids: a key sensory role in parasite signalling and development? Cellular
1210 microbiology. 2009;11(5):710-8. doi: 10.1111/j.1462-5822.2009.01295.x. PubMed PMID: 19207727.
1211 85. Morales MA, Pescher P, Spath GF. Leishmania major MPK7 protein kinase activity inhibits
1212 intracellular growth of the pathogenic amastigote stage. Eukaryotic cell. 2010;9(1):22-30. doi:
1213 10.1128/EC.00196-09. PubMed PMID: 19801421; PubMed Central PMCID: PMC2805286.

1214 86. Potenza M, Schenkman S, Laverriere M, Tellez-Inon MT. Functional characterization of
1215 TcCYC2 cyclin from Trypanosoma cruzi. Experimental parasitology. 2012;132(4):537-45. doi:
1216 10.1016/j.exppara.2012.09.002. PubMed PMID: 22982808.
1217 87. Dacher M, Morales MA, Pescher P, Leclercq O, Rachidi N, Prina E, Cayla M, Descoteaux A,
1218 Spath GF. Probing druggability and biological function of essential proteins in Leishmania combining
1219 facilitated null mutant and plasmid shuffle analyses. Molecular microbiology. 2014;93(1):146-66. doi:
1220 10.1111/mmi.12648. PubMed PMID: 24823804.
1221 88. Cayla M, Rachidi N, Leclercq O, Schmidt-Arras D, Rosenqvist H, Wiese M, Spath GF.
1222 Transgenic analysis of the Leishmania MAP kinase MPK10 reveals an auto-inhibitory mechanism
1223 crucial for stage-regulated activity and parasite viability. PLoS pathogens. 2014;10(9):e1004347. doi:
1224 10.1371/journal.ppat.1004347. PubMed PMID: 25232945; PubMed Central PMCID: PMC4169501.
1225 89. Jones NG, Thomas EB, Brown E, Dickens NJ, Hammarton TC, Mottram JC. Regulators of
1226 Trypanosoma brucei cell cycle progression and differentiation identified using a kinome-wide RNAi
1227 screen. PLoS pathogens. 2014;10(1):e1003886. doi: 10.1371/journal.ppat.1003886. PubMed PMID:
1228 24453978; PubMed Central PMCID: PMC3894213.
1229 90. Rachidi N, Taly JF, Durieu E, Leclercq O, Aulner N, Prina E, Pescher P, Notredame C, Meijer
1230 L, Spath GF. Pharmacological assessment defines Leishmania donovani casein kinase 1 as a drug target
1231 and reveals important functions in parasite viability and intracellular infection. Antimicrobial agents
1232 and chemotherapy. 2014;58(3):1501-15. doi: 10.1128/AAC.02022-13. PubMed PMID: 24366737;
1233 PubMed Central PMCID: PMC3957854.
1234 91. Baker N, Catta-Preta CMC, Neish R, Sadlova J, Powell B, Alves-Ferreira EVC, Geoghegan V,
1235 Carnielli JBT, Newling K, Hughes C, Vojtkova B, Anand J, Mihut A, Walrad PB, Wilson LG, Pitchford
1236 JW, Volf P, Mottram JC. Systematic functional analysis of Leishmania protein kinases identifies
1237 regulators of differentiation or survival. Nature communications. 2021;12(1):1244. doi:
1238 10.1038/s41467-021-21360-8. PubMed PMID: 33623024; PubMed Central PMCID: PMC7902614.
1239 92. Cayla M, Nievas YR, Matthews KR, Mottram JC. Distinguishing functions of trypanosomatid
1240 protein kinases. Trends in parasitology. 2022;38(11):950-61. doi: 10.1016/j.pt.2022.08.009. PubMed
1241 PMID: 36075845.
1242 93. Avila CC, Mule SN, Rosa-Fernandes L, Viner R, Barison MJ, Costa-Martins AG, Oliveira GS,
1243 Teixeira MMG, Marinho CRF, Silber AM, Palmisano G. Proteome-Wide Analysis of Trypanosoma
1244 cruzi Exponential and Stationary Growth Phases Reveals a Subcellular Compartment-Specific
1245 Regulation. Genes. 2018;9(8). doi: 10.3390/genes9080413. PubMed PMID: 30111733; PubMed
1246 Central PMCID: PMC6115888.
1247 94. Fritz M, Vanselow J, Sauer N, Lamer S, Goos C, Siegel TN, Subota I, Schlosser A, Carrington
1248 M, Kramer S. Novel insights into RNP granules by employing the trypanosome's microtubule skeleton
1249 as a molecular sieve. Nucleic acids research. 2015;43(16):8013-32. doi: 10.1093/nar/gkv731. PubMed
1250 PMID: 26187993; PubMed Central PMCID: PMC4652759.
1251 95. Cargnello M, Roux PP. Activation and function of the MAPKs and their substrates, the MAPK-
1252 activated protein kinases. Microbiology and molecular biology reviews : MMBR. 2011;75(1):50-83.
1253 doi: 10.1128/MMBR.00031-10. PubMed PMID: 21372320; PubMed Central PMCID: PMC3063353.
1254 96. Erdmann M, Scholz A, Melzer IM, Schmetz C, Wiese M. Interacting protein kinases involved
1255 in the regulation of flagellar length. Molecular biology of the cell. 2006;17(4):2035-45. doi:
1256 10.1091/mbc.e05-10-0976. PubMed PMID: 16467378; PubMed Central PMCID: PMC1415332.
1257 97. Zinoviev A, Leger M, Wagner G, Shapira M. A novel 4E-interacting protein in Leishmania is
1258 involved in stage-specific translation pathways. Nucleic acids research. 2011;39(19):8404-15. doi:
1259 10.1093/nar/gkr555. PubMed PMID: 21764780; PubMed Central PMCID: PMC3201875.
1260 98. Shrivastava R, Tupperwar N, Drory-Retwitzer M, Shapira M. Deletion of a Single LeishIF4E-
1261 3 Allele by the CRISPR-Cas9 System Alters Cell Morphology and Infectivity of Leishmania. mSphere.
1262 2019;4(5). doi: 10.1128/mSphere.00450-19. PubMed PMID: 31484740; PubMed Central PMCID:
1263 PMC6731530.
1264 99. Tupperwar N, Shrivastava R, Shapira M. LeishIF4E1 Deletion Affects the Promastigote
1265 Proteome, Morphology, and Infectivity. mSphere. 2019;4(6). doi: 10.1128/mSphere.00625-19.
1266 PubMed PMID: 31722993; PubMed Central PMCID: PMC6854042.
1267 100. Tupperwar N, Shrivastava R, Baron N, Korchev O, Dahan I, Shapira M. Characterization of an
1268 Atypical eIF4E Ortholog in Leishmania, LeishIF4E-6. International journal of molecular sciences.

2021;22(23). doi: 10.3390/ijms222312720. PubMed PMID: 34884522; PubMed Central PMCID: PMC8657474.
101. Baron N, Purushotham R, Pullaiahgari D, Bose P, Zarivach R, Shapira M. LeishIF4E2 is a cap-binding protein that plays a role in Leishmania cell cycle progression. FASEB journal : official publication of the Federation of American Societies for Experimental Biology. 2024;38(1):e23367. doi: 10.1096/fj.202301665R. PubMed PMID: 38095329.
102. Baird TD, Wek RC. Eukaryotic initiation factor 2 phosphorylation and translational control in metabolism. Advances in nutrition. 2012;3(3):307-21. doi: 10.3945/an.112.002113. PubMed PMID: 22585904; PubMed Central PMCID: PMC3649462.
103. Sloan KE, Warda AS, Sharma S, Entian KD, Lafontaine DLJ, Bohnsack MT. Tuning the ribosome: The influence of rRNA modification on eukaryotic ribosome biogenesis and function. RNA biology. 2017;14(9):1138-52. doi: 10.1080/15476286.2016.1259781. PubMed PMID: 27911188; PubMed Central PMCID: PMC5699541.
104. Imami K, Milek M, Bogdanow B, Yasuda T, Kastelic N, Zauber H, Ishihama Y, Landthaler M, Selbach M. Phosphorylation of the Ribosomal Protein RPL12/uL11 Affects Translation during Mitosis. Molecular cell. 2018;72(1):84-98 e9. doi: 10.1016/j.molcel.2018.08.019. PubMed PMID: 30220558.
105. Merrick WC, Pavitt GD. Protein Synthesis Initiation in Eukaryotic Cells. Cold Spring Harbor perspectives in biology. 2018;10(12). doi: 10.1101/cshperspect.a033092. PubMed PMID: 29735639; PubMed Central PMCID: PMC6280705.
106. Piazzi M, Bavelloni A, Gallo A, Faenza I, Blalock WL. Signal Transduction in Ribosome Biogenesis: A Recipe to Avoid Disaster. International journal of molecular sciences. 2019;20(11). doi: 10.3390/ijms20112718. PubMed PMID: 31163577; PubMed Central PMCID: PMC6600399.
107. Jungers CF, Elliff JM, Masson-Meyers DS, Phiel CJ, Origanti S. Regulation of eukaryotic translation initiation factor 6 dynamics through multisite phosphorylation by GSK3. The Journal of biological chemistry. 2020;295(36):12796-813. doi: 10.1074/jbc.RA120.013324. PubMed PMID: 32703900; PubMed Central PMCID: PMC7476728.
108. Janin M, Coll-SanMartin L, Esteller M. Disruption of the RNA modifications that target the ribosome translation machinery in human cancer. Molecular cancer. 2020;19(1):70. doi: 10.1186/s12943-020-01192-8. PubMed PMID: 32241281; PubMed Central PMCID: PMC7114786.
109. Bohlen J, Roiuk M, Teleman AA. Phosphorylation of ribosomal protein S6 differentially affects mRNA translation based on ORF length. Nucleic acids research. 2021;49(22):13062-74. doi: 10.1093/nar/gkab1157. PubMed PMID: 34871442; PubMed Central PMCID: PMC8682771.
110. Khoshnevis S, Dreggors-Walker RE, Marchand V, Motorin Y, Ghalei H. Ribosomal RNA 2'-O-methylations regulate translation by impacting ribosome dynamics. Proceedings of the National Academy of Sciences of the United States of America. 2022;119(12):e2117334119. doi: 10.1073/pnas.2117334119. PubMed PMID: 35294285; PubMed Central PMCID: PMC8944910.
111. Das T, Shin SC, Song EJ, Kim EE. Regulation of Deubiquitinating Enzymes by Post-Translational Modifications. International journal of molecular sciences. 2020;21(11). doi: 10.3390/ijms21114028. PubMed PMID: 32512887; PubMed Central PMCID: PMC7312083.
112. Wang F, Ning S, Yu B, Wang Y. USP14: Structure, Function, and Target Inhibition. Frontiers in pharmacology. 2021;12:801328. doi: 10.3389/fphar.2021.801328. PubMed PMID: 35069211; PubMed Central PMCID: PMC8766727.
113. Gonzalez J, Ramalho-Pinto FJ, Frevert U, Ghiso J, Tomlinson S, Scharfstein J, Corey EJ, Nussenzweig V. Proteasome activity is required for the stage-specific transformation of a protozoan parasite. The Journal of experimental medicine. 1996;184(5):1909-18. doi: 10.1084/jem.184.5.1909. PubMed PMID: 8920878; PubMed Central PMCID: PMC2192890.
114. Bijlmakers MJ. Ubiquitination and the Proteasome as Drug Targets in Trypanosomatid Diseases. Frontiers in chemistry. 2020;8:630888. doi: 10.3389/fchem.2020.630888. PubMed PMID: 33732684; PubMed Central PMCID: PMC7958763.
115. Wiese M. Leishmania MAP kinases--familiar proteins in an unusual context. International journal for parasitology. 2007;37(10):1053-62. doi: 10.1016/j.ijpara.2007.04.008. PubMed PMID: 17548090.
116. Cardoso J, Soares MJ, Menna-Barreto RF, Le Bloas R, Sotomaior V, Goldenberg S, Krieger MA. Inhibition of proteasome activity blocks Trypanosoma cruzi growth and metacyclogenesis.

1323 Parasitology research. 2008;103(4):941-51. doi: 10.1007/s00436-008-1081-6. PubMed PMID:
1324 18581141.
1325 117. Cardoso J, Lima Cde P, Leal T, Gradia DF, Fragoso SP, Goldenberg S, De Sa RG, Krieger MA.
1326 Analysis of proteasomal proteolysis during the in vitro metacyclogenesis of Trypanosoma cruzi. PloS
1327 one. 2011;6(6):e21027. doi: 10.1371/journal.pone.0021027. PubMed PMID: 21698116; PubMed
1328 Central PMCID: PMC3117861.
1329 118. Munoz C, San Francisco J, Gutierrez B, Gonzalez J. Role of the Ubiquitin-Proteasome Systems
1330 in the Biology and Virulence of Protozoan Parasites. BioMed research international.
1331 2015;2015:141526. doi: 10.1155/2015/141526. PubMed PMID: 26090380; PubMed Central PMCID:
1332 PMC4452248.
1333 119. Hunter T. The age of crosstalk: phosphorylation, ubiquitination, and beyond. Molecular cell.
1334 2007;28(5):730-8. doi: 10.1016/j.molcel.2007.11.019. PubMed PMID: 18082598.
1335 120. Nguyen LK, Kolch W, Kholodenko BN. When ubiquitination meets phosphorylation: a systems
1336 biology perspective of EGFR/MAPK signalling. Cell communication and signaling : CCS. 2013;11:52.
1337 doi: 10.1186/1478-811X-11-52. PubMed PMID: 23902637; PubMed Central PMCID: PMC3734146.
1338 121. Barbour H, Nkwe NS, Estavoyer B, Messmer C, Gushul-Leclaire M, Villot R, Uriarte M,
1339 Boulay K, Hlayhel S, Farhat B, Milot E, Mallette FA, Daou S, Affar EB. An inventory of crosstalk
1340 between ubiquitination and other post-translational modifications in orchestrating cellular processes.
1341 iScience. 2023;26(5):106276. doi: 10.1016/j.isci.2023.106276. PubMed PMID: 37168555; PubMed
1342 Central PMCID: PMC10165199.
1343 122. Waddington CH. Canalization of development and genetic assimilation of acquired characters.
1344 Nature. 1959;183(4676):1654-5. doi: 10.1038/1831654a0. PubMed PMID: 13666847.
1345

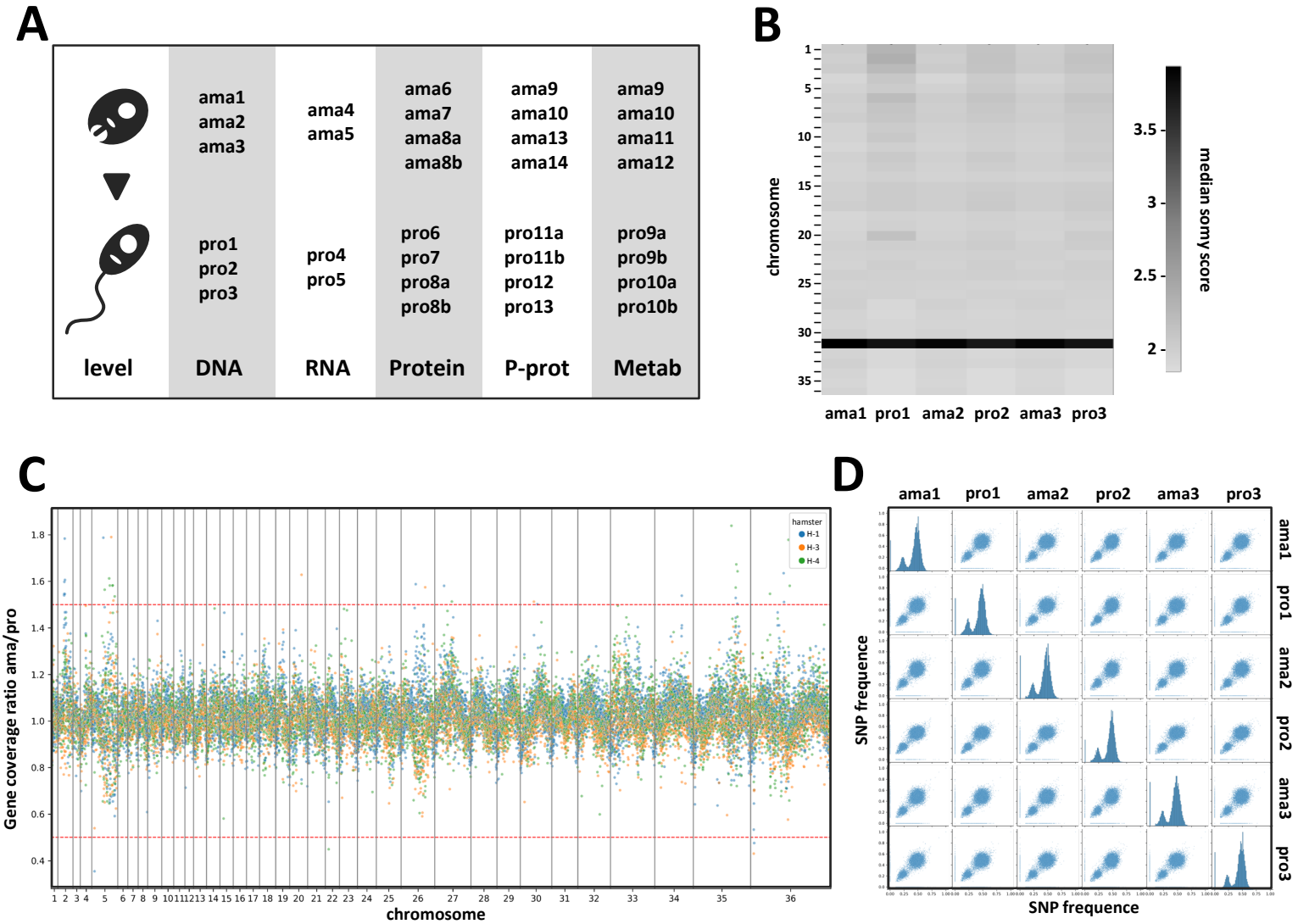
A
ama1
ama2
ama3
ama4
ama5
ama6
ama7
ama8a
ama8b
ama9
ama10
ama13
ama14
ama9
ama10
ama11
ama12
pro1
pro2
pro3
pro4
pro5
pro6
pro7
pro8a
pro8b
pro11a
pro11b
pro12
pro13
pro9a
pro9b
pro10a
pro10b
level
DNA
RNA
Protein
P-prot
Metab
B
chromosome
median somy score
ama1 pro1 ama2 pro2 ama3 pro3
C
Gene coverage ratio ama/pro
chromosome
hamster
H-1
H-3
H-4
D
ama1 pro1 ama2 pro2 ama3 pro3
SNP frequence
SNP frequence

Figure 1

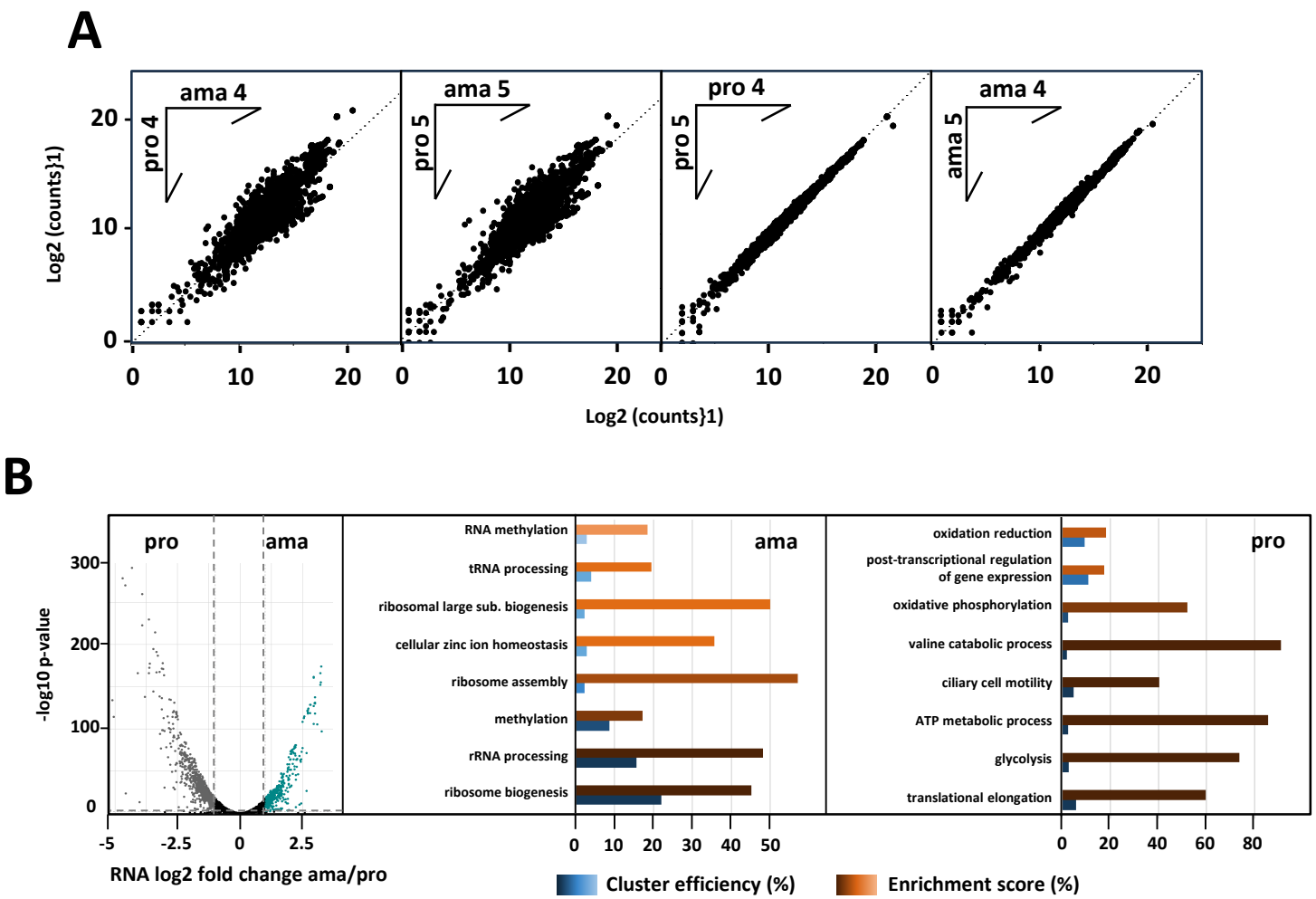
A
ama 4
pro 4
ama 5
pro 5
pro 4
pro 5
ama 4
ama 5
Log2 (counts}1)
Log2 (counts}1)
B
pro
ama
-log10 p-value
RNA log2 fold change ama/pro
ama
RNA methylation
tRNA processing
ribosomal large sub. biogenesis
cellular zinc ion homeostasis
ribosome assembly
methylation
rRNA processing
ribosome biogenesis
pro
oxidation reduction
post-transcriptional regulation of gene expression
oxidative phosphorylation
valine catabolic process
ciliary cell motility
ATP metabolic process
glycolysis
translational elongation
Cluster efficiency (%)
Enrichment score (%)

Figure 2

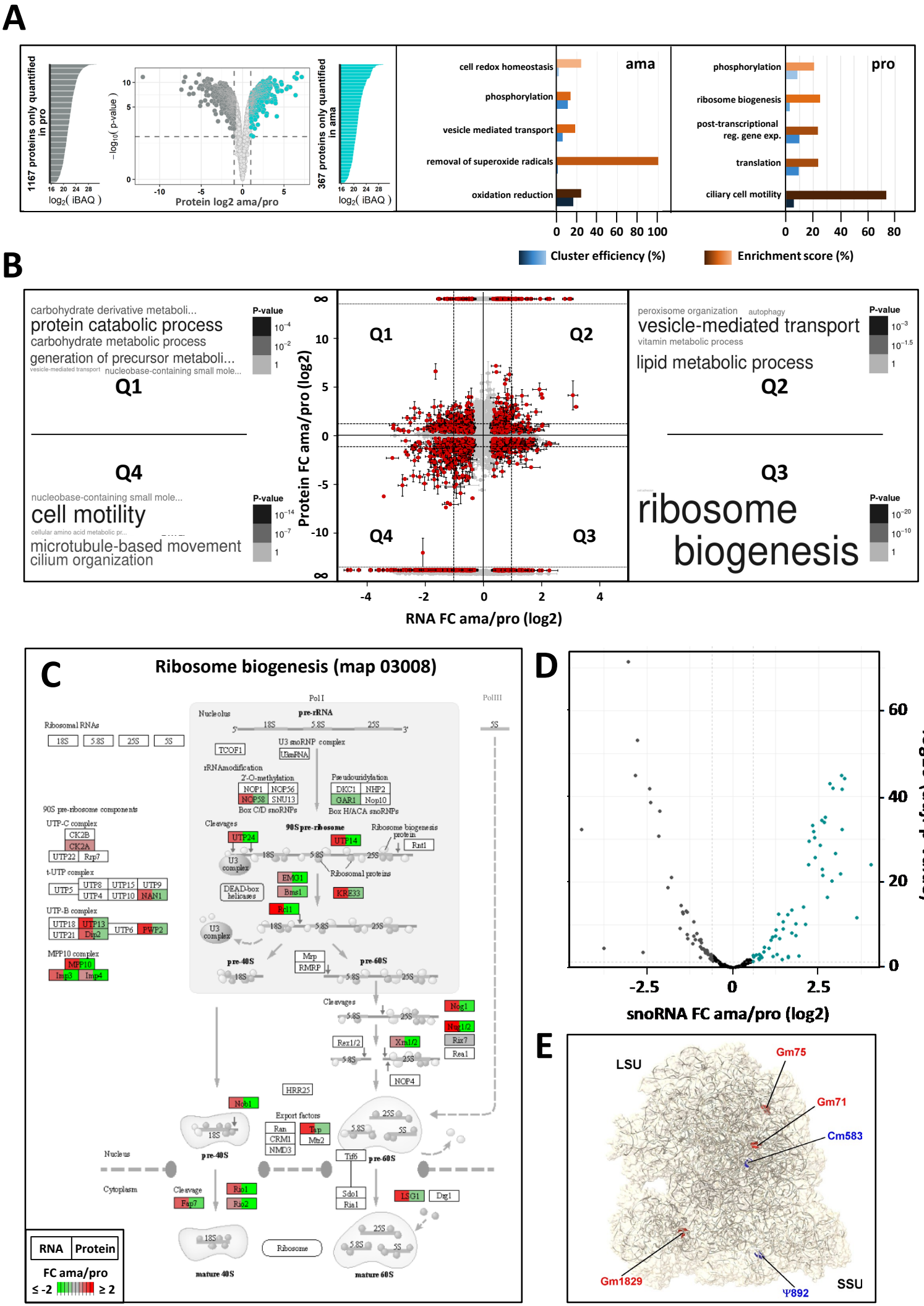
A
1167 proteins only quantified in pro
log2(iBAQ)
−log10(p-value)
Protein log2 ama/pro
367 proteins only quantified in ama
log2(iBAQ)
ama
cell redox homeostasis
phosphorylation
vesicle mediated transport
removal of superoxide radicals
oxidation reduction
pro
phosphorylation
ribosome biogenesis
post-transcriptional reg. gene exp.
translation
ciliary cell motility
Cluster efficiency (%)
Enrichment score (%)
B
carbohydrate derivative metaboli...
protein catabolic process
carbohydrate metabolic process
generation of precursor metaboli...
vesicle-mediated transport
nucleobase-containing small mole...
Q1
P-value
Q2
peroxisome organization
autophagy
vesicle-mediated transport
vitamin metabolic process
lipid metabolic process
Q4
nucleobase-containing small mole...
cell motility
microtubule-based movement
cilium organization
Q3
ribosome biogenesis
Protein FC ama/pro (log2)
RNA FC ama/pro (log2)
C
Ribosome biogenesis (map 03008)
Ribosomal RNAs
90S pre-ribosome components
UTP-C complex
t-UTP complex
UTP-B complex
MPP10 complex
Nucleolus
pre-rRNA
U3 snoRNP complex
rRNA modification
2'-O-methylation
Pseudouridylation
Box C/D snoRNPs
Box H/ACA snoRNPs
Cleavages
90S pre-ribosome
Ribosome biogenesis protein
Ribosomal proteins
DEAD-box helicases
pre-40S
pre-60S
Export factors
Nucleus
Cytoplasm
Cleavage
mature 40S
mature 60S
Ribosome
RNA
Protein
FC ama/pro
≤ -2
≥ 2
D
-log10 (adj. p-value)
snoRNA FC ama/pro (log2)
E
LSU
Gm75
Gm71
Cm583
Gm1829
Ψ892
SSU

Figure 3

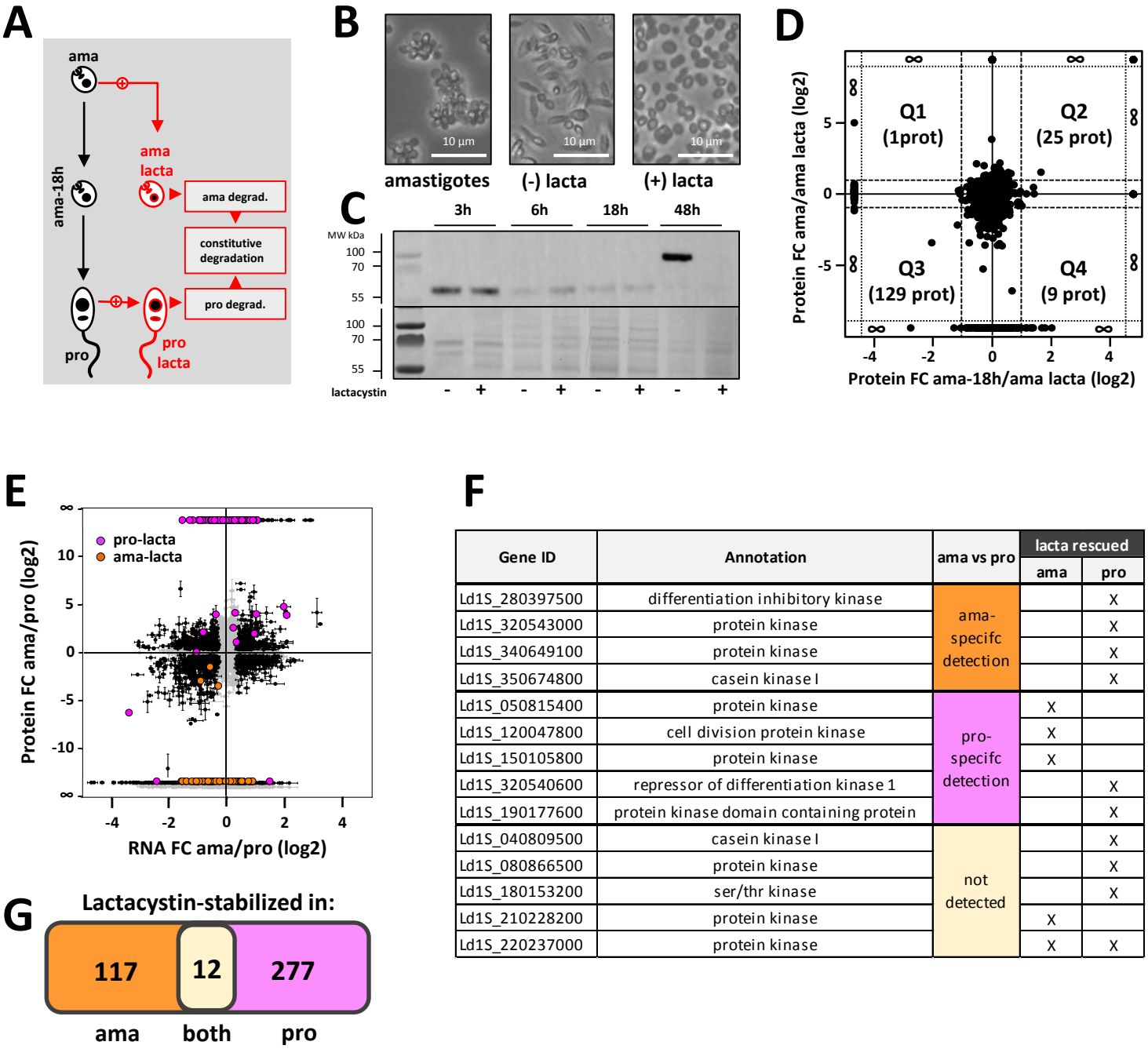

F

Gene ID	Annotation	ama vs pro	lacta rescued	
			ama	pro
Ld1S_280397500	differentiation inhibitory kinase	ama-specifc detection		X
Ld1S_320543000	protein kinase			X
Ld1S_340649100	protein kinase			X
Ld1S_350674800	casein kinase I			X
Ld1S_050815400	protein kinase	pro-specifc detection	X	
Ld1S_120047800	cell division protein kinase		X	
Ld1S_150105800	protein kinase		X	
Ld1S_320540600	repressor of differentiation kinase 1			X
Ld1S_190177600	protein kinase domain containing protein			X
Ld1S_040809500	casein kinase I	not detected		X
Ld1S_080866500	protein kinase			X
Ld1S_180153200	ser/thr kinase			X
Ld1S_210228200	protein kinase		X	
Ld1S_220237000	protein kinase		X	X

Figure 4

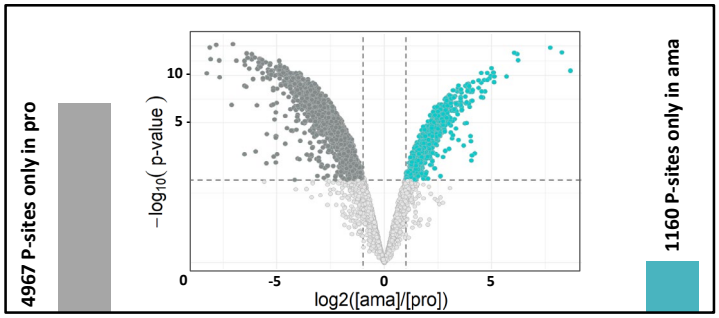
A
4967 P-sites only in pro
1160 P-sites only in ama
−log10(p-value)
log2([ama]/[pro])

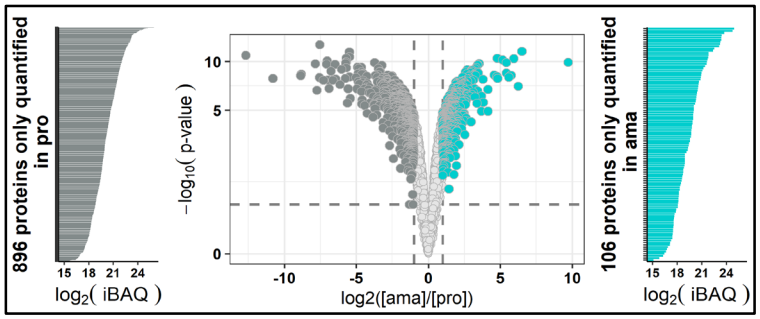
896 proteins only quantified in pro
106 proteins only quantified in ama
−log10(p-value)
log2([ama]/[pro])
log2(iBAQ)

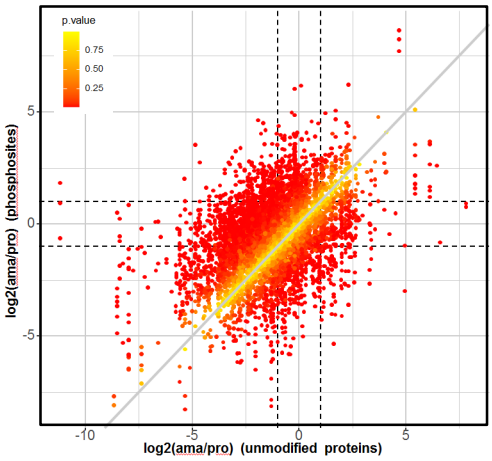
B
p.value
0.75
0.50
0.25
log2(ama/pro) (phosphosites)
log2(ama/pro) (unmodified proteins)

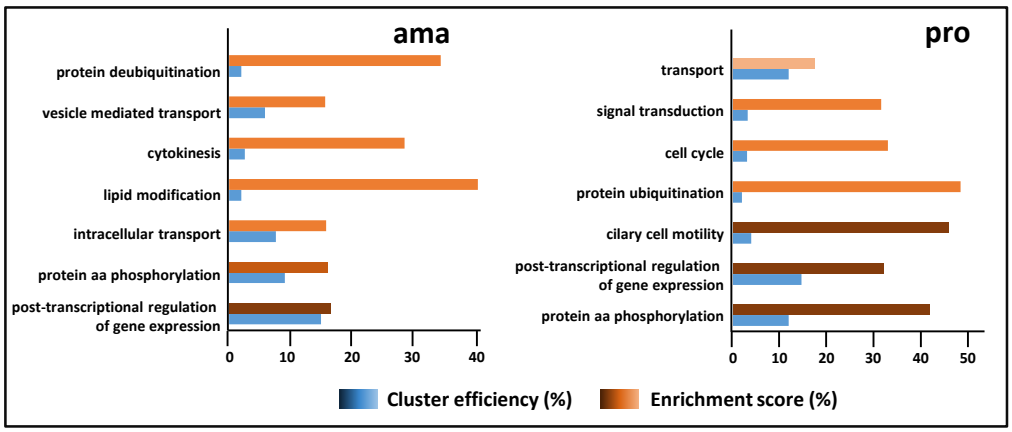
C
ama
protein deubiquitination
vesicle mediated transport
cytokinesis
lipid modification
intracellular transport
protein aa phosphorylation
post-transcriptional regulation of gene expression
pro
transport
signal transduction
cell cycle
protein ubiquitination
cilary cell motility
post-transcriptional regulation of gene expression
protein aa phosphorylation
Cluster efficiency (%)
Enrichment score (%)

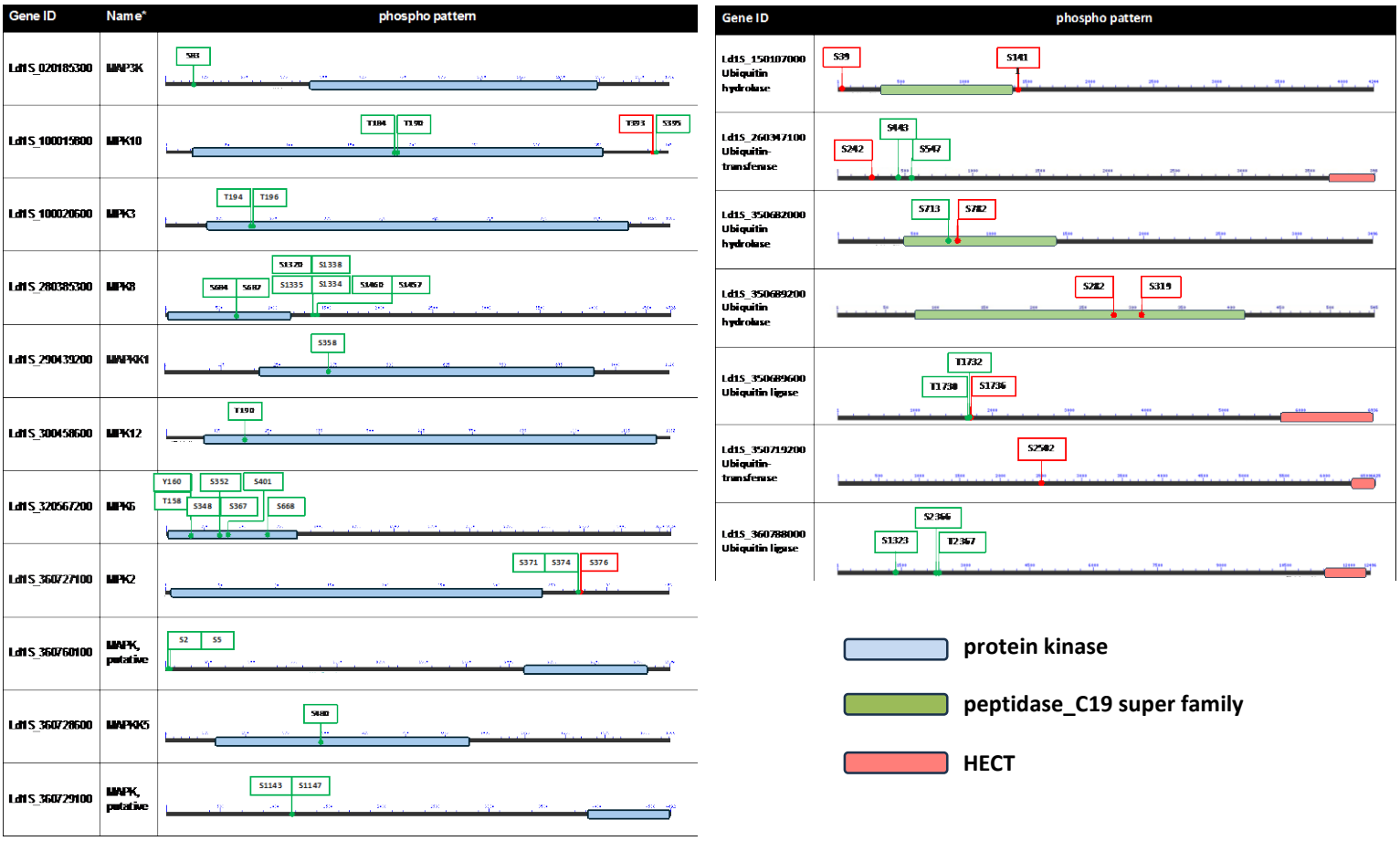
D
Gene ID
Name*
phospho pattern
Ld1S_02085300
Ld1S_10001800
Ld1S_10002600
Ld1S_28038300
Ld1S_29043200
Ld1S_30045600
Ld1S_32056700
Ld1S_36072700
Ld1S_36076010
Ld1S_36072800
Ld1S_36072900
Ld1S_15010700
Ld1S_26034700
Ld1S_35068200
Ld1S_35068900
Ld1S_35068960
Ld1S_35071900
Ld1S_36078800
protein kinase
peptidase_C19 super family
HECT

Figure 5

A
Recursive regulation
Signaling
Translation
RNA turnover
ama
pro
Metabolic retooling
Stage-adapted ribosomes
Stage-specific networks
Flagellar biogenesis
Kinases <> proteasome
Kinases <> phosphatases
Kinases <> ribosome
Reciprocal regulation
B
ama
Protein ubiquitination
Protein deubiquitination
MAP kinase cascade
Protein kinase
Protein linked to ub./deubiquitination
Protein linked to ribosome
C
pro
Protein kinase
Protein linked to ub./deubiquitination
Protein linked to ribosome
Ribosome biogenesis
Ribosomal protein
MAP kinase cascade
Proteasome mediated proteolysis

Figure 6

Supp Figures

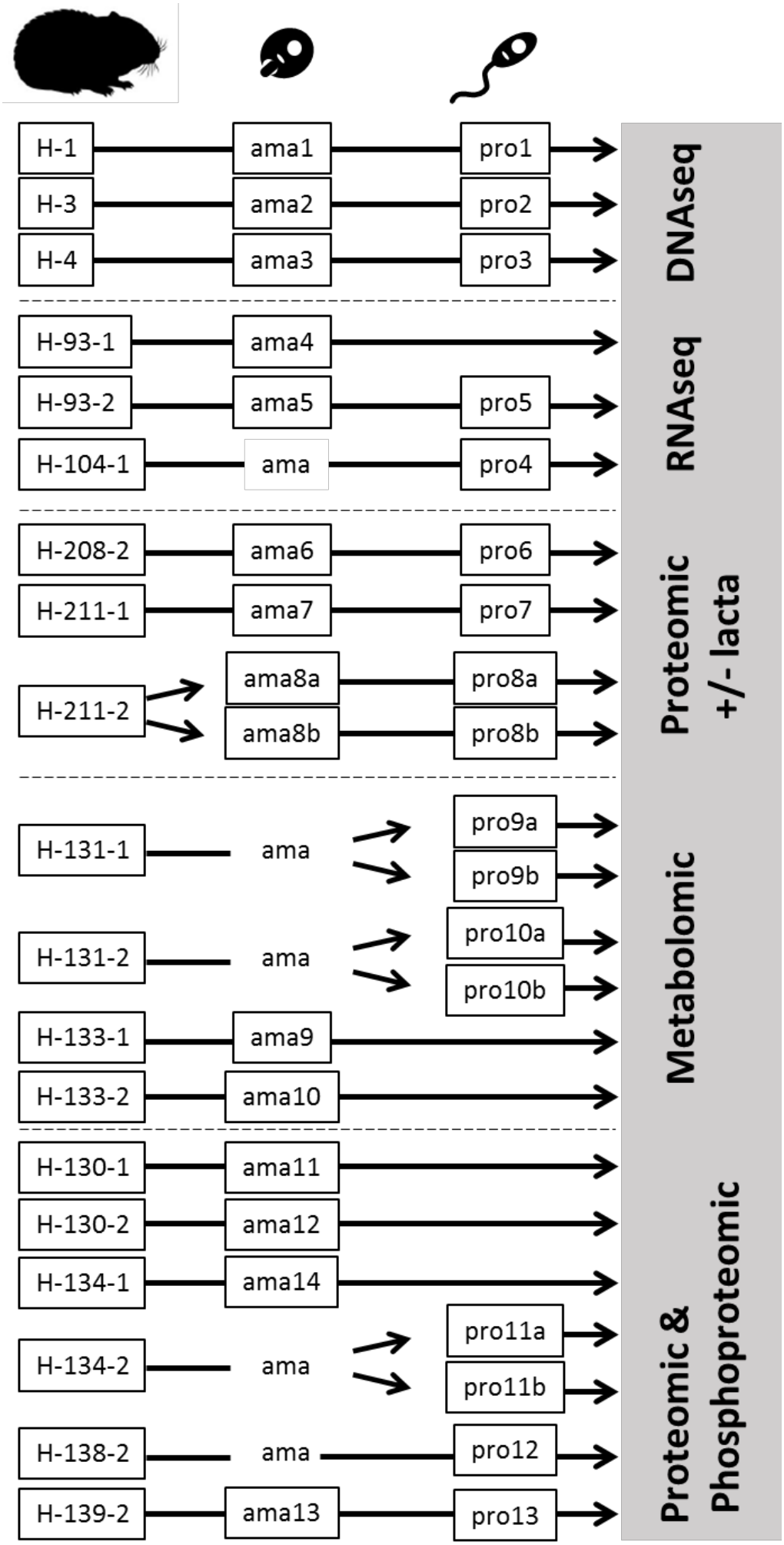

Sup Figure S1

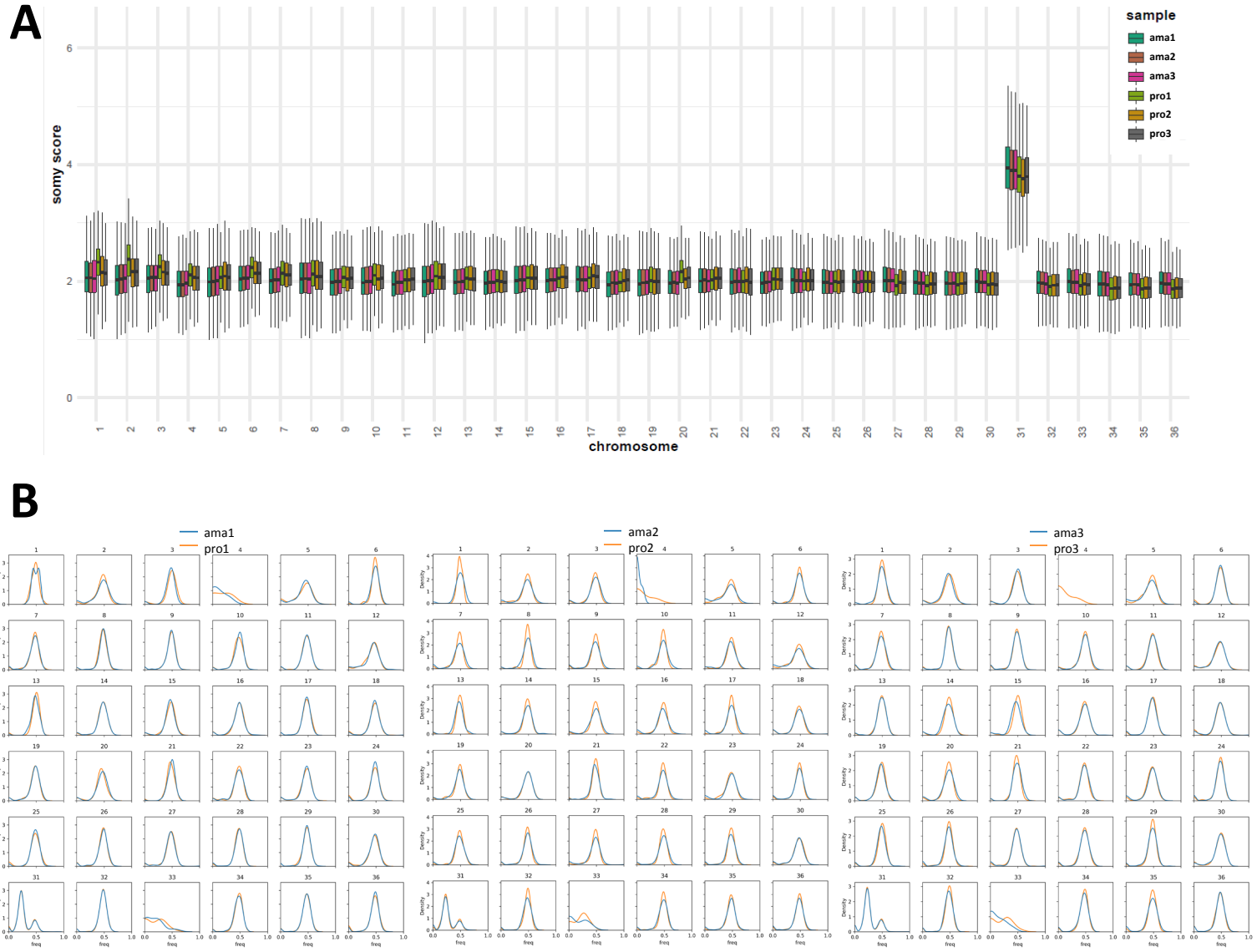

Sup Figure S2

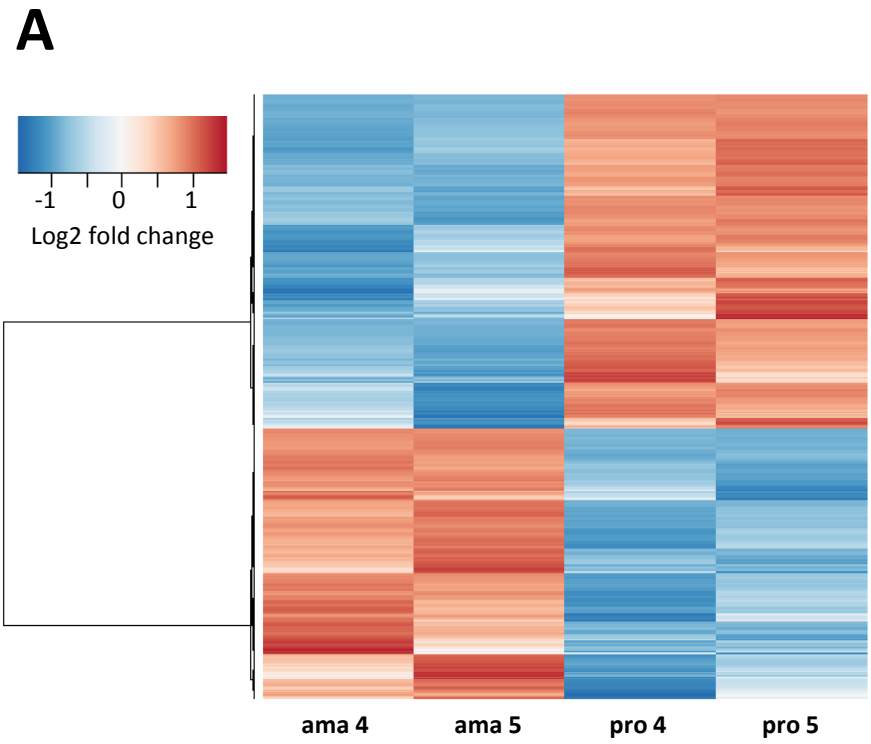

Sup Figure S3

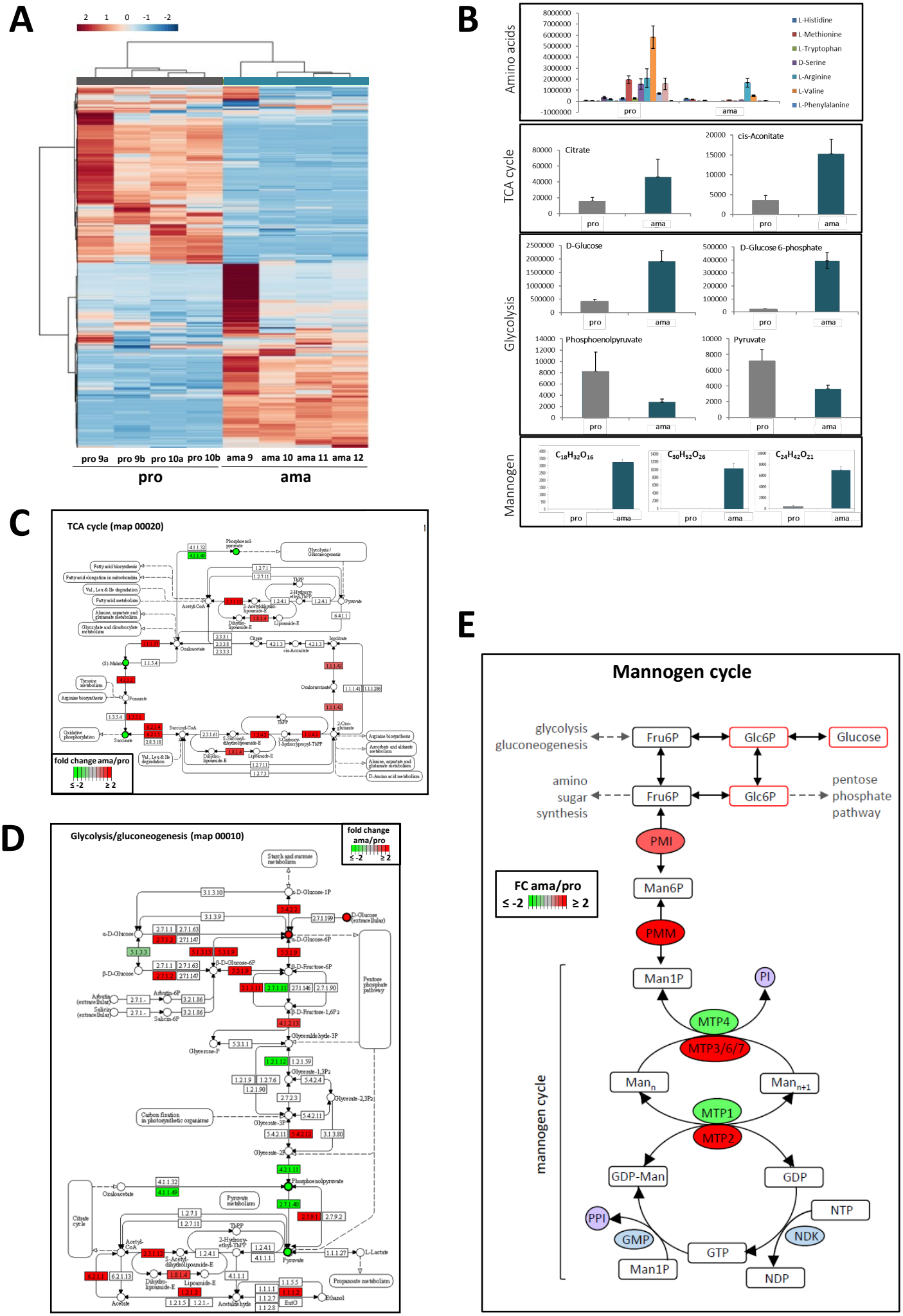

Sup Figure S4

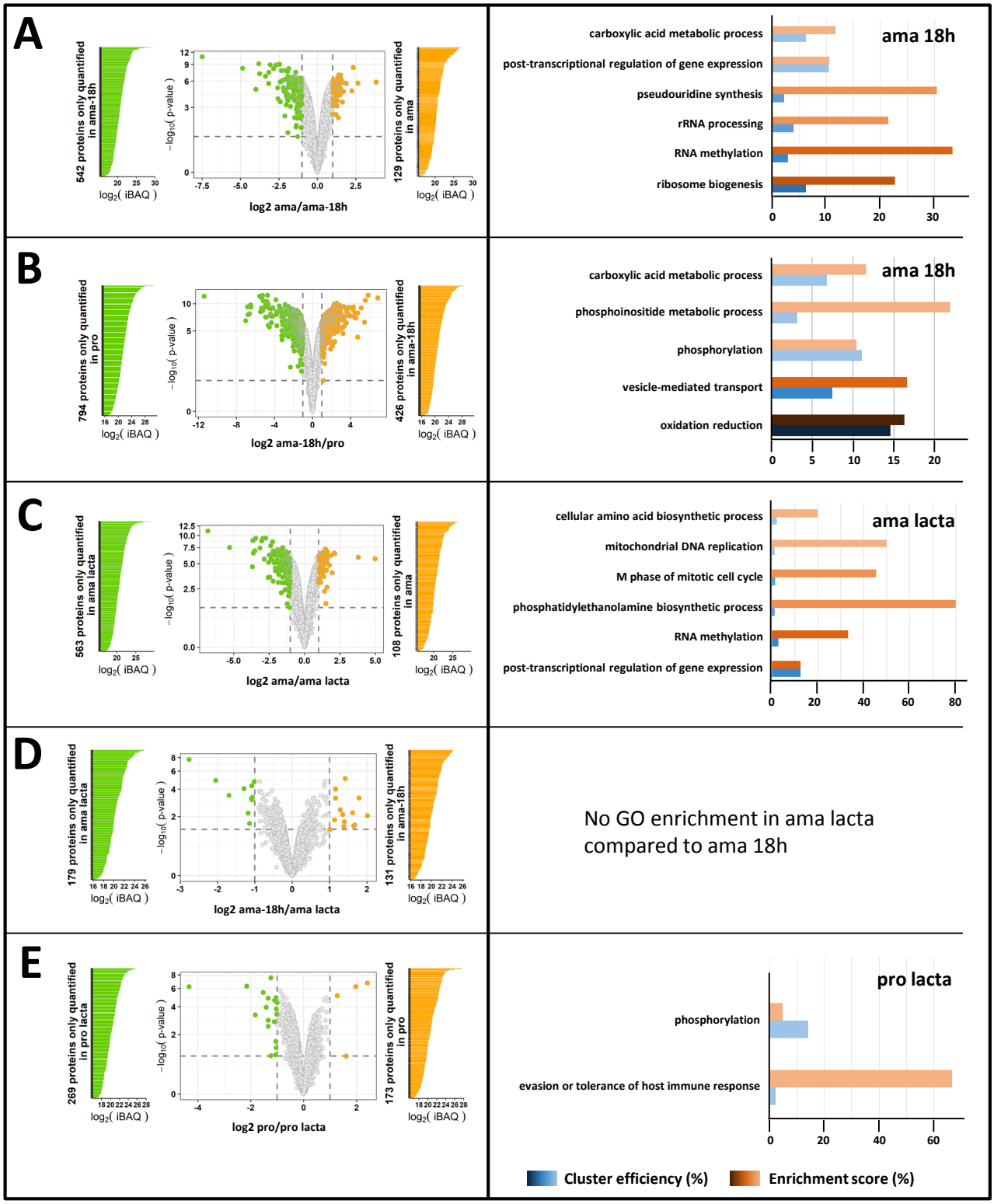

Sup Figure S5

A

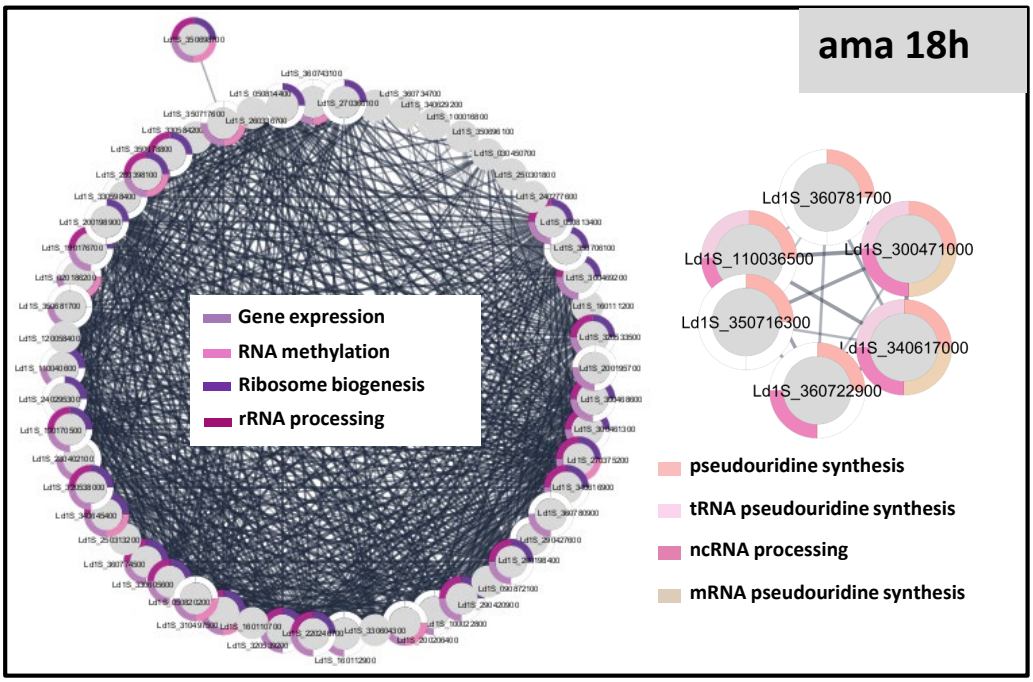

B

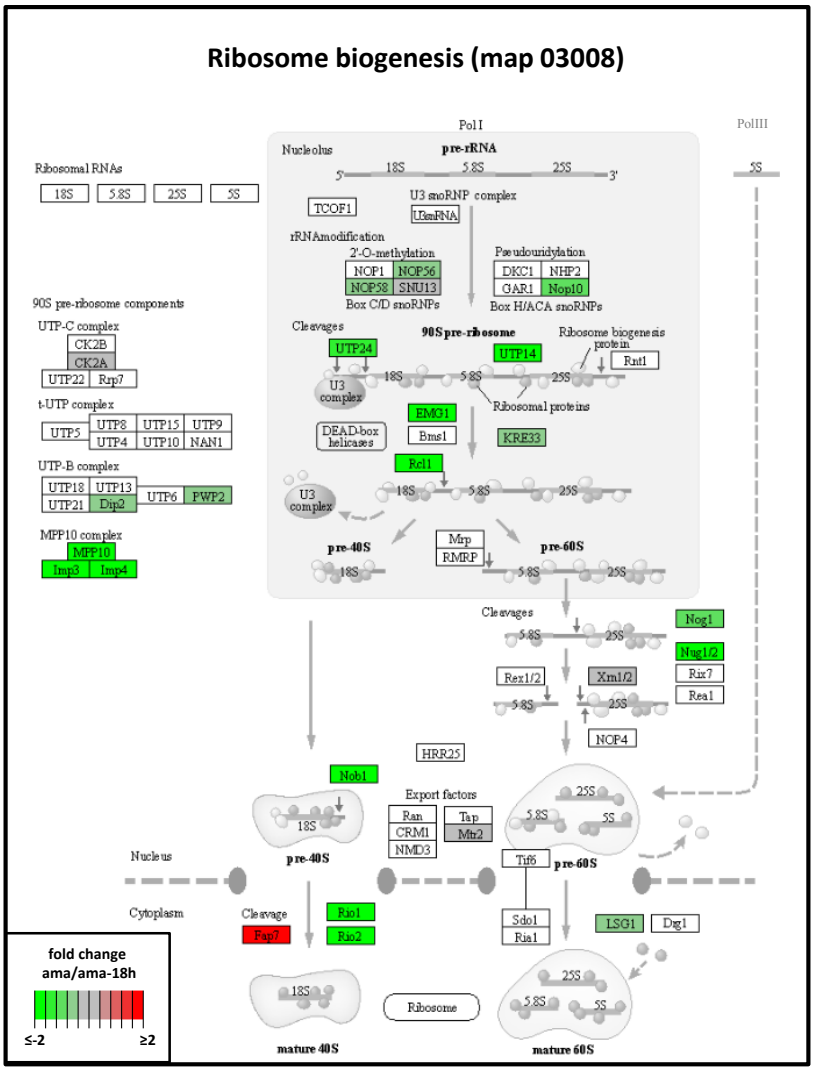

Sup Figure S6

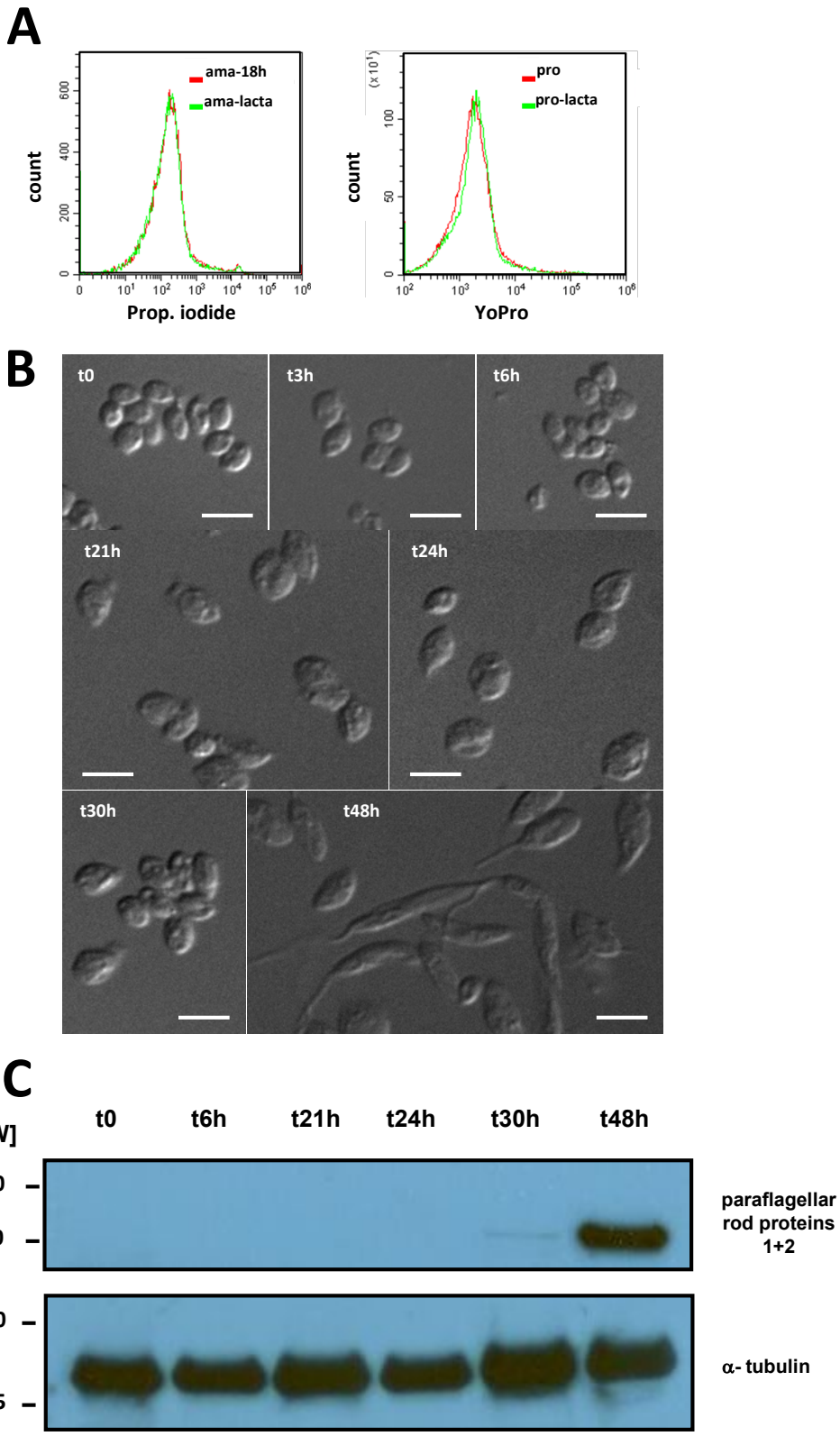

Sup Figure S7

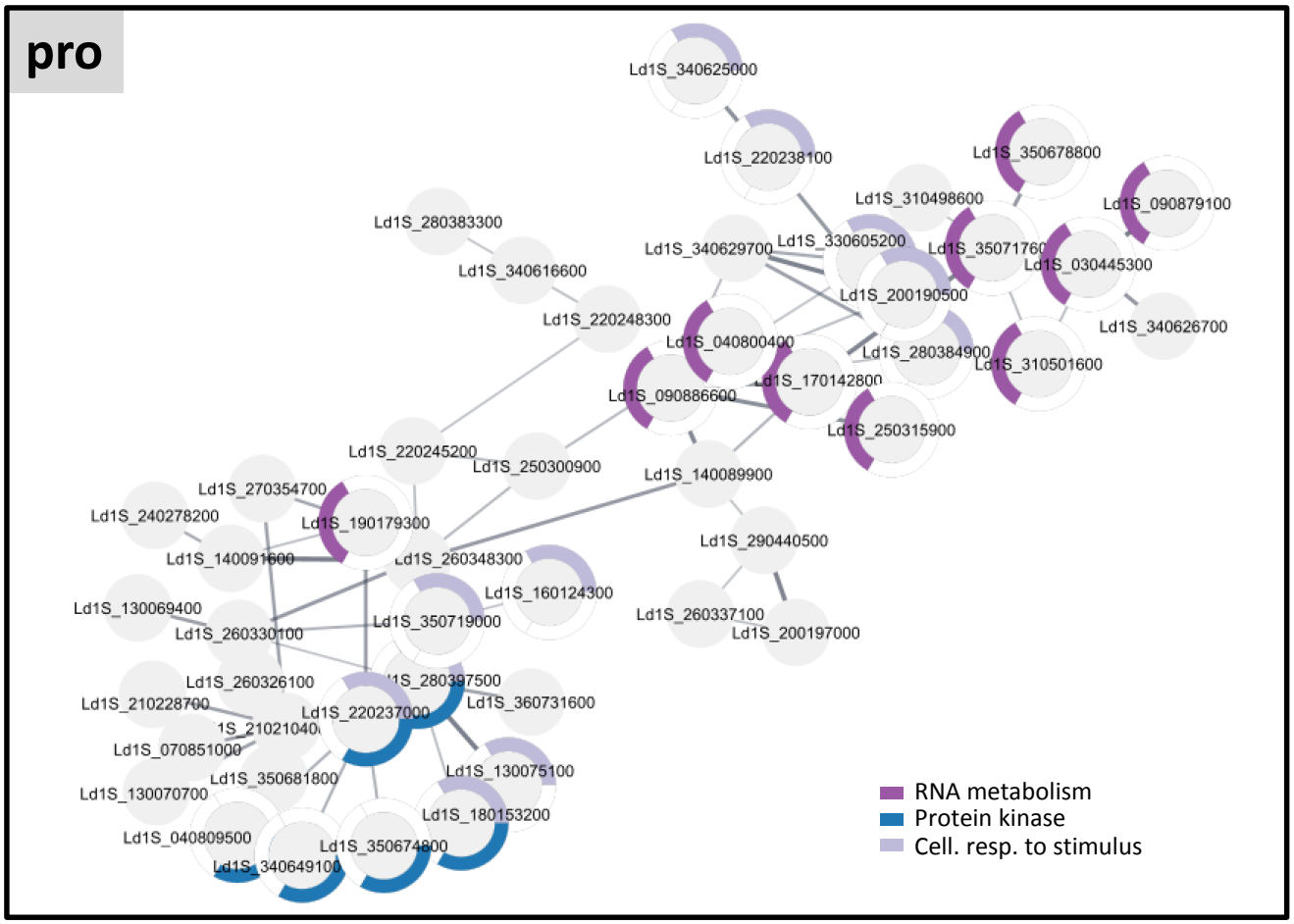

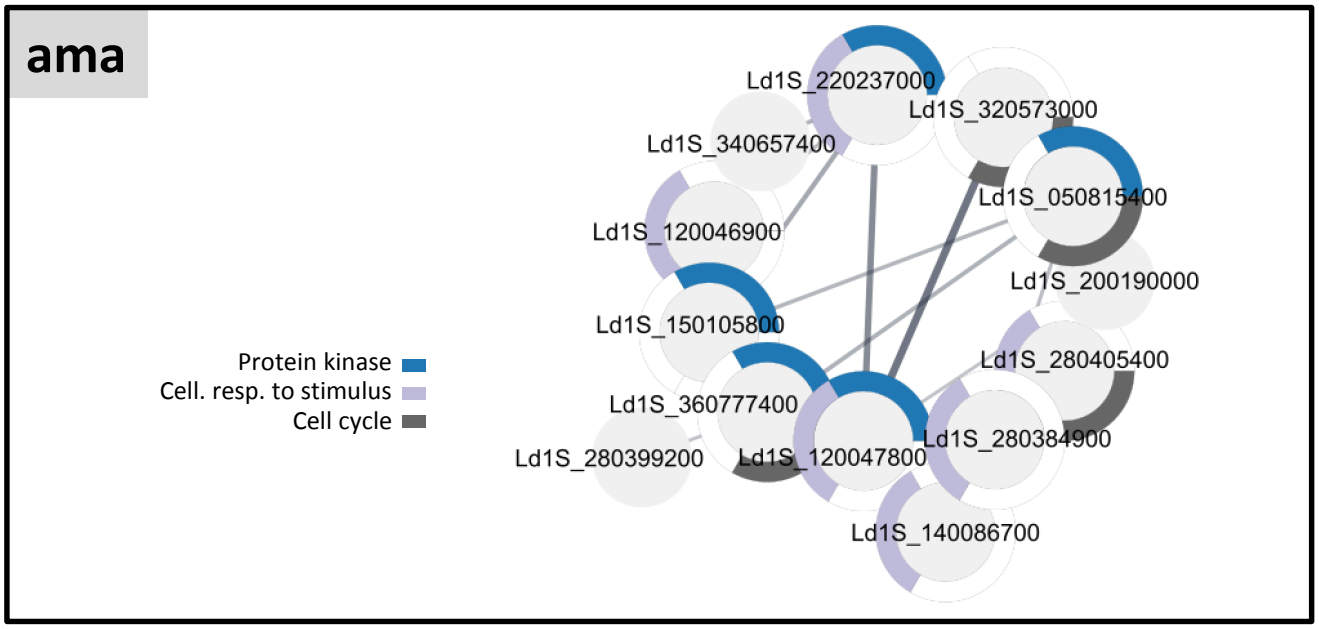

Sup Figure S8

ID Ld1S	ID LdBPK	ID LmxM	Annotation	KO phenotype*
Ld1S_320540600	LdBPK_320860.1	LmxM.31.0810.1	Repressor of differentiation kinase 1, RDK1	Loss of fitness during pro to ama differentiation Loss of fitness in animal infection
Ld1S_220244300	LdBPK_220970.1	LmxM.22.1150.1	Protein kinase domain containing protein, putative	
Ld1S_190177600	LdBPK_191290.1	LmxM.19.1300	hypothetical protein, unknown function (PP: Protein kinase domain containing protein, putative)	
Ld1S_180153200	LdBPK_180650.1	LmxM.07.0900	serine/threonine kinase-like protein, putative	
Ld1S_080866500	LdBPK_080870.1	LmxM.08.0930.1	protein kinase, putative	
Ld1S_040809500	LdBPK_041230.1	LmxM.04.1210.1	casein kinase I, putative	
Ld1S_350674800	LdBPK_351020.1	LmxM.34.1000.1	casein kinase I, putative	
Ld1S_340649100	LdBPK_342850.1	LmxM.33.3020.1	protein kinase, putative	Loss of fitness in animal infection
Ld1S_320543000	LdBPK_321080.1	LmxM.31.1020.1	protein kinase, putative	
Ld1S_280397500	LdBPK_281800.1	LmxM.28.1670.1	differentiation inhibitory kinase, putative, ZFK	Moderate loss of fitness in animal infection
Ld1S_220237000	LdBPK_220370.1	LmxM.22.0490.1	protein kinase, putative	ESSENTIAL
Ld1S_210228200	LdBPK_210330.1	LmxM.21.0270.1	protein kinase, putative	Loss of fitness in animal infection
Ld1S_150105800	LdBPK_151180.1	LmxM.15.1200	protein kinase, putative	
Ld1S_120047800	LdBPK_120130.1	LmxM.12.0130.1	Cell division protein kinase, putative	
Ld1S_050815400	LdBPK_050550.1	LmxM.05.0550.1	protein kinase, putative	

Baker et al

Sup Figure S9

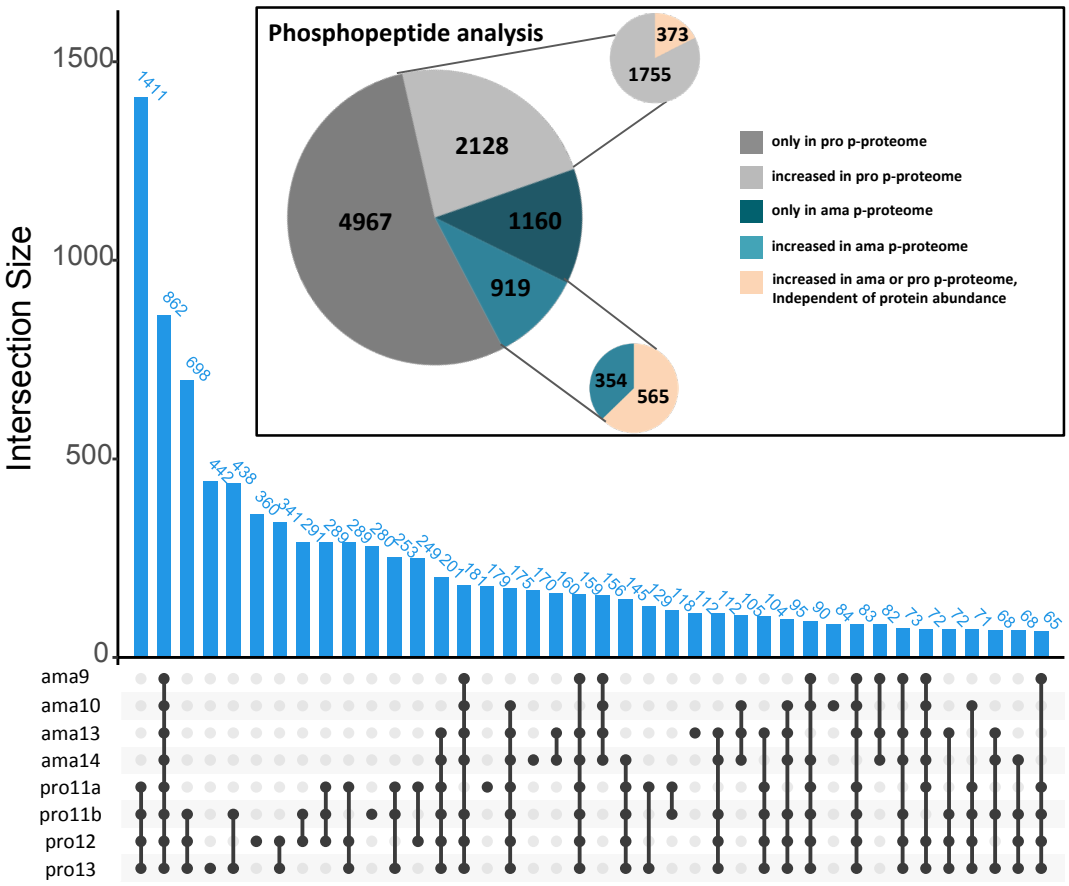

Sup Figure S10

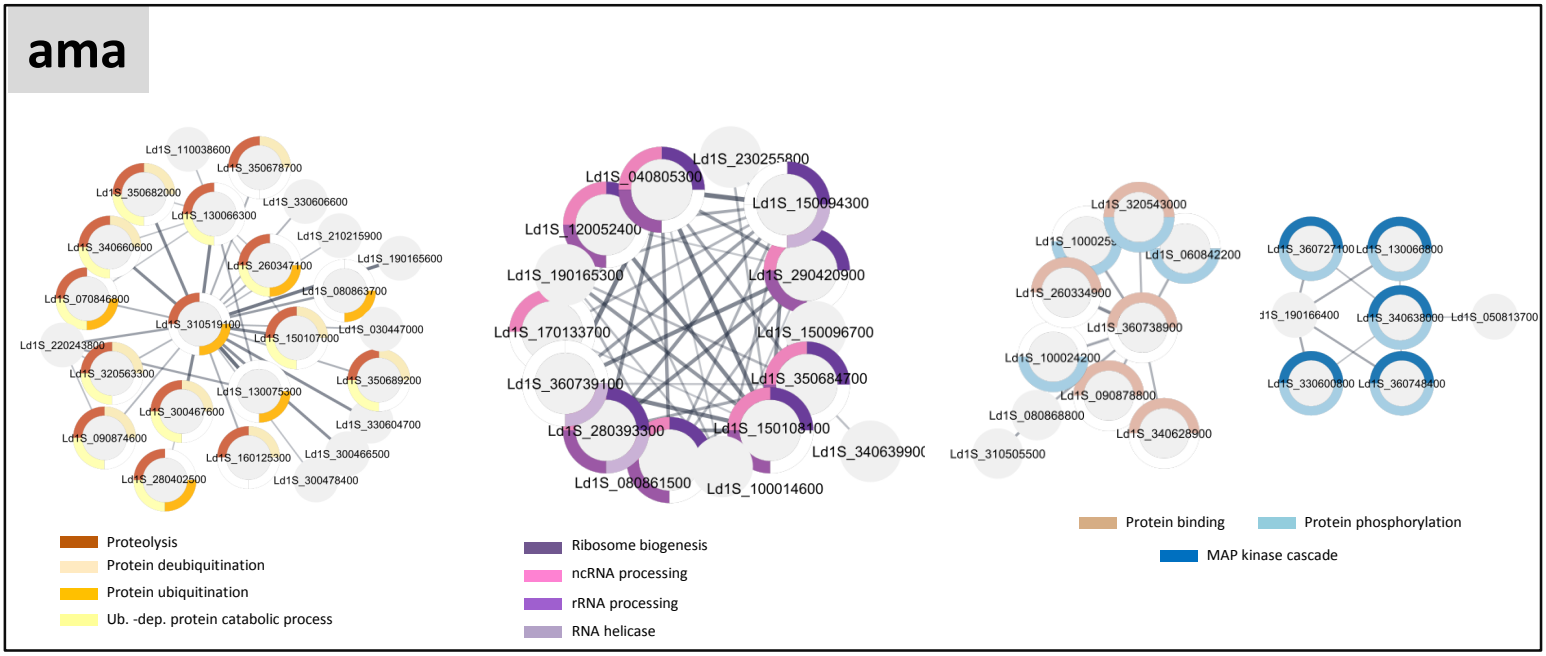

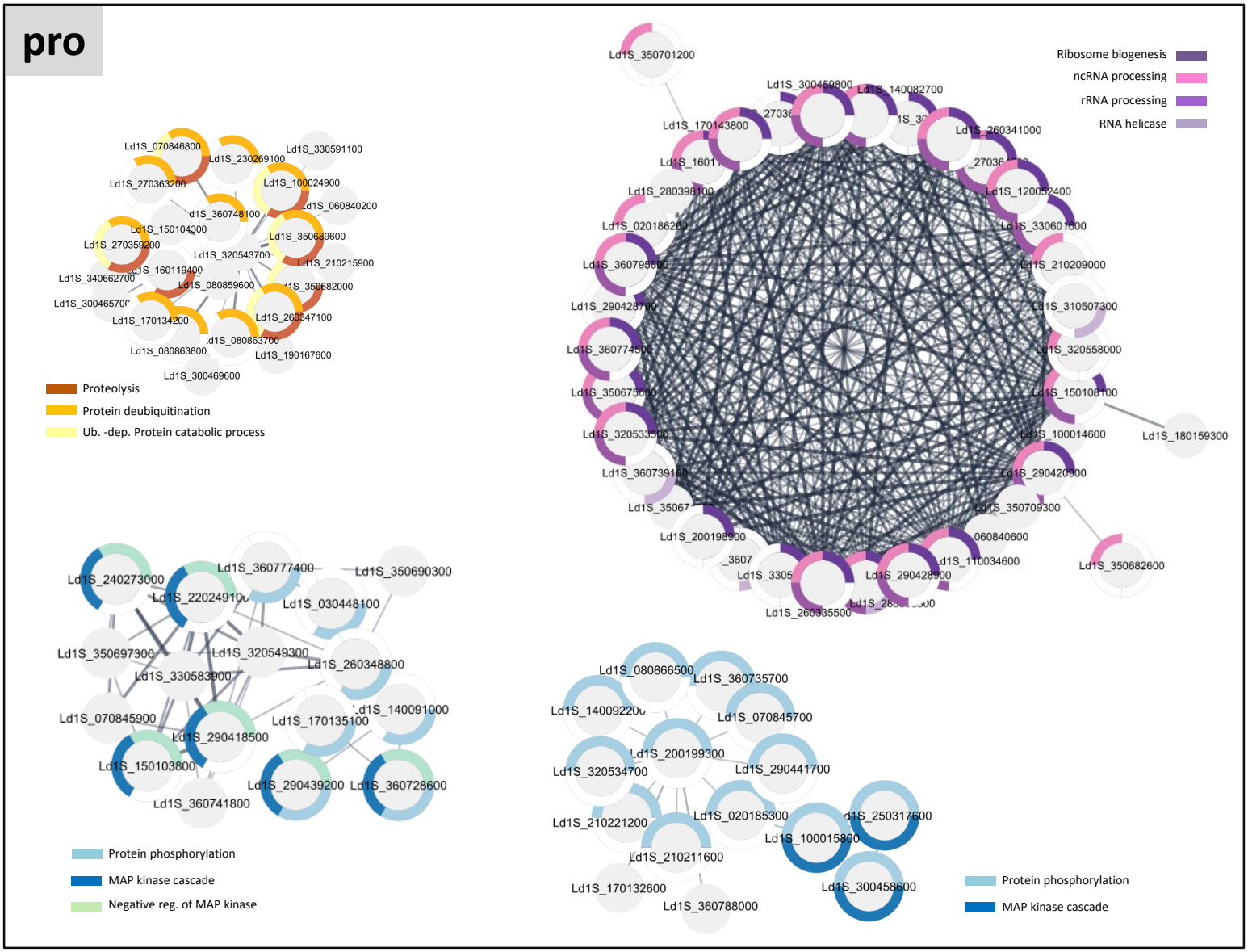

Sup Figure S11